Title:

- Structural basis of CO_2 valence coding in Drosophila

Authors:

Example: Javorski Dominik[1], Bergkirchner Beate[1], Ensinger Gernot[1], Lingl Alexander[1], Navolic Jelena[2], Batawi Ashwaq[3], Hummel Thomas[1]

Affiliations:

[1]Department of Neurosciences and Development, University of Vienna, Djerassiplatz 1, 1030 Vienna, Austria

[2]Center for Molecular Neurobiology Hamburg, University Medical Center Hamburg-Eppendorf, Falkenried 94, 20251 Hamburg, Germany

[3]King Abdulaziz University, 21589 Jeddah, Saudi Arabia

*Corresponding author: Email: thomas.hummel@univie.ac.at

Abstract

In the olfactory system, glomerular sensory channels of single receptor identity support reliable odor recognition for appropriate approach or avoidance behaviors. For many olfactory stimuli, the assigned sensory value is innate but weighted by the internal state and previous experiences. How context-dependent modulation of innate valence coding supports distinct behavioral responses is poorly understood. Here we show that CO_2 sensory information in Drosophila, intrinsically aversive but modified by attractive food signals, diverges from the canonical glomerular channel already in the antennal lobe via the polarized local interneuron LN23. LN23 relays sensory input via an extraglomerular CO_2 pathway and manipulation of LN23 activity revealed a dominant role in CO_2-induced avoidance behavior. The extraglomerular CO_2 pathway projects to the posterior lateral protocerebrum (PLP) adjacent to the canonical Lateral Horn (LH) olfactory processing center and segregates into anatomically distinct valence channels. Connectome data together with functional characterization showed the convergence of parallel CO_2 channels onto two interconnected 3rd order neurons which integrate additional sensory modalities via distinct mechanisms: while the glomerular CO_2 pathway converge with food relay neurons onto separated dendritic domains of the PD5 interneuron in the LH, the extraglomerular pathways integrating CO_2 information with antennal humidity and temperature modalities establish antagonistic inputs onto the PLP interneuron PV9. This early anatomical divergence of a defined olfactory channel

followed by separated multimodal integration provides a structural basis for context-dependent valence coding and appropriate behavioral responses.

56 **Introduction**

57 The ability to recognize and react to environmental stimuli is essential for the survival of
58 animals. Insect olfactory systems allow the sensing and integration of volatile signals to
59 identify food resources and avoid potential threats (Wilson, 2013). Although CO_2 is a
60 component of the atmosphere, local changes in ambient CO_2 levels can induce context-
61 dependent behavioral responses (Faucher et al. 2006; Hansson & Stensmyr, 2011). Walking
62 Drosophila show robust CO_2 induced avoidance (Suh et al. 2004; Kwon et al. 2007; Faucher et
63 al. 2006), while in more aroused states such as flight or foraging, CO_2 becomes an attractive
64 olfactory cue (van Breugel et al. 2018) which is linked to dopamine levels affecting mushroom
65 body output neurons (Lewis et al. 2015; Sachse & Beshel 2016). At the circuit level, prolonged
66 CO_2 exposure leads to olfactory habituation, mediated by plasticity of GABAergic interneurons
67 in the antennal lobe (Das et al. 2011; Olsen & Wilson, 2008; Nagel & Wilson, 2016; Sachse et
68 al. 2007; Semelidou et al. 2018). Interestingly, Drosophila avoidance behavior directly
69 correlates with the activity of CO_2 specific olfactory receptor neurons (MacWilliam et al. 2018),
70 raising the question of how CO_2-induced sensory activity is transformed into central valence
71 representations and modulated to support context-dependent behavior (Frechter et al. 2019).

72 The peripheral CO_2 circuit follows the canonical organization of olfactory sensory channels. A
73 single population of ORNs (ab1C) co-express the gustatory receptors Gr21a and Gr63a and
74 projects ipsilaterally to the V glomerulus in the ventral antennal lobe (Suh et al. 2004; Kwon
75 et al. 2007; Vosshall and Stocker 2007). CO_2 sensation is transmitted to higher brain centers
76 through two glomerular PNv types: a bilateral cholinergic PN (PNv^{bi}) projecting to both the
77 Mushroom Body (MB) and Lateral Horn (LH), and a LH specific relay via a unilateral PN (PNv^{uni})
78 (Grabe et al., 2016; Lin et al. 2013; Sachse et al. 2007; Tanaka et al. 2012). Although distinct
79 spatial LH domains encoding opposite hedonic values and odor intensity have been identified
80 (Frechter et al. 2019; Das Chakraborty et al. 2022), glomerular PNs provide synaptic input to a
81 diverse set of LH neurons making the identification of central brain representation and
82 context-dependent modulation of a given sensory channel difficult (Dolan et al. 2019; Scheffer
83 et al. 2020).

84 Here we describe the identification of novel CO_2 relay channel, morphologically and
85 functionally separate from the canonical glomerular circuit via a polarized olfactory

86 interneuron, LN23. The LN23 pathway mediates a robust CO_2-induced aversion largely
87 unaffected by glomerular circuit plasticity but allows early multimodal integration.
88 Furthermore, the parallel pathways of glomerular and extraglomerular PNs converge onto a
89 small group of LH interneurons as a core domain for CO_2 valence coding in the central brain.

90 **Material and Methods**
91

92 **Drosophila Stocks**
93

94 VT031497 (PNv^{bi} Gal4 and the alternative line: R53A05; BDSC#38859; BDSC: Bloomington
95 Drosophila Stock Center), NP7273 (PNv^{uni} Gal4), R44A02 (LN23 Gal4; BDSC#50196) were used
96 to target neurons PNv^{bi}, PNv^{uni} and LN23 respectively. LN23-lexA (BDSC#53644) and PNv^{bi}-lexA
97 (VT031497 lexA) were used in sybGRASP (BDSC#93197 / reverse direction BDSC#64315) and
98 tGRASP (BDSC#79040/reverse direction BDSC#79039) experiments to express the
99 postsynaptic GFP fragment. Gr21-Gal4 (BDSC#57600) was used to target ORNs which project
100 specifically to the V-glomerulus. To target LNv1 and LNv2, we used NP1227P from the Max
101 Planck Institute and NP2426-P from the Kyoto Stock Center. The Gal4 driver line BDSC #40444
102 was used for l2LN19. UAS-shibire^{ts} (Gift from Barry Dickson) was used to inhibit neurons at
103 restrictive 31°C. UAS-ReaCh (BDSC#53741) was used in optogenetic experiments to artificially
104 activate specific neuronal subsets which are labelled by the Gal4 lines. CantonS and w1118
105 wildtype flies were used for control experiments. The Gr63a^1 (BDSC#9941) mutant stock was
106 used in the behavior experiments as control for flies which are unable to detect CO_2. In
107 addition to our main LN23 line (BDSC#50196) an additional line also labeling LN23
108 (BDSC#48408) was used for optogenetics. UAS-CaLexA (BDSC#66542) was used in
109 combination with the Gal4 lines to label active neurons. To further activate or silence
110 specifically active neurons a CaLexA stock without GFP was used (BDSC#66543) in combination
111 with lexAop-ReaCh or lexAop-shi^{ts} respectively. *UAS-DenMark::cherry* was used to label
112 dendrites of neurons while *UAS-syb::GFP* and *UAS-syt::GFP* specifically labeled presynaptic
113 terminals. To confirm the location of active T-bars in LN23 and PNv^{bi} neurons, we also applied
114 *UAS-brp::GFP* (BDSC#36291 and BDSC#36292).

115

116

117 **Immunohistochemistry**

118

119 Flies were dissected in PBS (phosphate buffer solution) and brains were fixed in 2% PFA
120 (Paraformaldehyde). After the fixation brains were washed 3 times with 0.3% PBT (phosphate
121 buffer with TritonX) and then blocked with Goat serum. After 1 hour of blocking the 1st AB
122 (Antibody) was applied and the brains were kept in a 4°C fridge overnight. The next day brains
123 were washed again 3 times before applying the 2nd AB. After the staining protocol was
124 complete, brains were mounted and afterwards scanned with a confocal microscope. Anti
125 Ncad rat (1:10, DHSB) was used to label all neuropiles in the fly brain in all experiments. For
126 CaLexA experiments anti GFP rabbit (1:5000, Invitrogen) was used additionally to enhance the
127 signal strength, according to Masuyama et al. (2012). GRASP experiments, DenMark and
128 labeling of presynaptic terminals (*syt::GFP* and *syb::GFP*) didn't require any antibodies besides
129 anti-Ncad since the endogenous signal was sufficient and changes after CO_2 incubation should
130 not be distorted. For MCFO, first Antibodies were Anti-Ncad rat (1:10) or Anti-ollas rat
131 (1:2000), Anti-flag mouse (1:2000) and Anti-HA rabbit (1:2000). As second antibodies anti-rat
132 647 (1:500), anti-mouse (highly cross-absorbed, 1:300) and anti-rabbit (1:500) were applied.

133 **MCFO (Multicolor flip-out)**

134

135 To label single cells in a usually rather broad expressing Gal4-line, we took advantage of a
136 method established by Nern et al. 2015, called MCFO. They recombined four constructs,
137 consisting of an UAS-site, followed by a stop-cassette to suppress transcription and one of
138 four different transmembrane proteins, which can, if expressed, be labeled via antibodies.
139 These four independent constructs can also be expressed together in the same cell, which
140 leads to a mixture of colors and increased probability of one cell getting labeled in one distinct
141 color. The stochastic excision of the stop cassette is achieved by a heat sensitive enzyme,
142 whose activation is triggered by incubating the flies at 37°C in a water bath.

143 **GRASP**

144

145 To visualize synaptic contacts two different GRASP tools were used. SybGRASP is activity
146 dependent because one fragment of GFP is located on vesicle membranes. As vesicles fuse

147 with the presynaptic membrane, which is dependent on incoming action potentials, the large
148 GFP fragment is exposed in the synaptic cleft and can reconstitute with the small GFP fragment
149 located on the postsynaptic membrane (Macpherson et al. 2015). tGRASP, or targeted GRASP
150 (Shearin et al. 2018), is activity independent and the two GFP fragments are bound to pre and
151 postsynaptic specific proteins (Cacophony and Telencephalin respectively). A comparison of
152 these two GRASP techniques allowed us to make assumptions about changes of synaptic
153 activity and changes to synaptic density. No antibodies against GFP were used since the
154 endogenous expression was sufficient. GFP intensities were quantified with FIJI, which is
155 measured as the mean gray value of a defined region of interest (ROI) above a threshold. To
156 subtract the mean grey value of the background noise, intensity was measured in another
157 glomerulus (same size of ROI) which was not showing any signal. Each datapoint in the
158 diagrams represents one quantified glomerulus. The same applies to intensity measurements
159 for the following two sections.

160 **DenMark::cherry / Syt:GFP, syb::GFP**
161

162 *UAS-syt::GFP* and *UAS-syb::GFP* were used to label presynaptic terminals of target neurons.
163 Synaptotagmin (*syt*) and synaptobrevin (*syb*) are proteins of the vesicle membrane and
164 therefore a Gal4 driven expression of the GFP tagged proteins shows strong signal in the
165 presynaptic terminals. *UAS-DenMark* (Dendritic Marker) is a somatodendritic marker (*cherry*)
166 to label dendrites. *GFP/Cherry* intensities were quantified with FIJI.

167 **CaLexA**
168

169 CaLexA (Masuyama et al. 2012) was used to label active cells. It is based on the NFAT
170 transcription factor, which is calcium responsive. As Ca^+ enters a cell, a chimeric lexA-VP16-
171 NFAT, enters the nucleus where expressed lexA can bind to lexAop inducing the expression of
172 GFP. The stronger and longer the excitation lasts, higher GFP intensities are expected. GFP
173 levels were quantified in FIJI as it was described in the section about GRASP. There was no
174 selection for gender and all flies tested were 2 days old at the start of the experiments. In the
175 experimental condition where flies were kept under the elevated level of 5% CO_2 the duration
176 of the exposure was 3 days. We also used a CaLexA construct where expressed lexA is not
177 expressing GFP but instead driving the expression of a temperature sensitive shibire protein
178 to silence neurons. Further we also used this stock in combination with lexA driven expression

179 of ReaCh to specifically further activate physiologically active neurons. 99% spermidine was
180 used as an inhibitor to GR21a receptors. 5yl were put on a small piece of cotton which was
181 then transferred to a vial containing the flies which were used in the experiments after 3 days
182 of exposure.

183 **Behavioral experiments**
184

185 For behavior experiments, flies were kept in total darkness, in 25°C incubators in vials
186 containing fly food. Flies which were used in optogenetics were raised on fly food containing
187 all-trans-retinal to enhance their response to light exposure (Vilinsky et al. 2018). All flies were
188 age matched and tested when they were 3-4 days old. Since there was no observed difference
189 between male and female flies both sexes were used in all behavioral experiments. As we did
190 not observe any behavioral artifacts caused by either green or red LED light we opted for the
191 green LEDs, since they elicited a stronger response in the flies (compared to Inagaki et al.,
192 2014).

193 Flies were immediately transferred to empty vials which can be connected to the CO_2 or
194 optogenetic setup after they were taken out of the incubators. The whole procedure was also
195 done in darkness (red light was used to be able to handle the flies, which is barely visible for
196 the flies) to minimize visual distraction affecting the fly's behavior. The whole apparatus was
197 shifted sideways, and the flies were gently moved to the elevator segment of the setup. The
198 elevator was lowered to a position short above the decision point and the flies were given 60
199 seconds rest. After the resting period either a green LED light or CO_2 flow was activated and
200 the elevator was lowered to the decision point.

201 The animals were given 20 seconds to move inside the behavioral setup and make a choice.
202 Afterwards the elevator was pulled up again, so that the flies remained in either the test tube,
203 control tube or the central elevator area. Each of these populations was counted and a
204 preference index (PI) calculated, that was defined as the percentage of flies located in the
205 control arm (air filled /dark) of the setup, minus the percentage of flies located in the test arm
206 (CO_2 filled/light). Since in some of the tested populations, a few animals remained in the
207 central elevator part of the arena, their decision was defined as neutral. Their number was
208 divided by two and added to both the test and control population for the PI. Each datapoint
209 in the diagrams represents the PI of a group of flies (n=15-40).

210

211 **Hemibrain analyses**

212

213 Connectivity data were obtained from the neuPrint interface (neuPrint, Janelia Research
214 Campus; https://neuprint.janelia.org/) built on the Hemibrain connectome (Scheffer et al.
215 2020). It was used to study and model the neurons involved in the V-circuit. The main goal
216 was to identify synaptic connectivity between the different layers of information processing
217 within the circuit. Finally, the putative circuit was reconstructed in 3D and PN/LN output zones
218 were identified. Neuronbridge.janelia.org was used to gather 3D images from l2_PNm17 and
219 sm_PNm1. FlyWire.ai was a tool to quickly get information about the predicted
220 neurotransmitter identities of neurons.

221 **Statistics**

222

223 All diagrams and statistical analyses were done by using GraphPad Prism 9 software. Normally
224 distributed data were compared with a student's t-test, whereas datasets that did not meet
225 normality assumptions were analyzed with a Mann–Whitney U test. Behavioral data spanning
226 multiple days were tested with a one-way ANOVA. Statistical significance is indicated in the
227 figures by asterisks, with $p < 0.05$ (*), $p < 0.01$ (**), $p < 0.001$ (***), and $p < 0.0001$ (****).

228

229 **Results**

230

231 **Glomerular circuit dynamics of CO_2 perception**

232

233 The V glomerulus at the ventral AL surface is innervated by a single population of about 40
234 CO_2-sensitive olfactory receptor neurons (ORNv) expressing the two gustatory receptors
235 GR21a and GR63a (Kwon et al. 2007; Jones et al. 2007) (Fig.1A-B). Each ORNv axon forms 3-5
236 terminal branches tightly packed in a non-overlapping fashion with other ORN terminals (Fig.
237 1, C-C´´), providing sensory input to glomerular inter- and projection neurons (Fig1D-G´)
238 (Grabe et al., 2016).

239 To identify relay neurons of the V glomerulus with different physiological properties we
240 screened a collection of Gal4 lines using the CaLexA activity reporter to compare intracellular
241 Ca^{2+} levels under ambient CO_2 conditions (Koyama et al. 2021; Masuyama et al. 2012) (Fig. 1H-
242 O). Gal4 lines for ORNv show strong CaLexA reporter activity (Fig.1H), in line with a high default
243 activity of CO_2-receptive sensory neurons due to the absence of $GABA_B$-mediated presynaptic
244 inhibition (MacWilliam et al. 2018; Olsen & Wilson, 2008; Root et al. 2008). In contrast to
245 elevated Ca^{2+} levels in ORNv, the two uniglomerular PN classes of the V glomerulus, unilateral
246 V_l2PNs (PNv^{uni}) and bilateral V_ilPNs (PNv^{bi}, Fig. 1D) do not show any significant level of
247 CaLexA activation under ambient air conditions (Fig. 1I, J). Two main classes of local
248 interneurons, LNv1 and LNv2 display moderate levels of CaLexA activity at atmospheric CO_2
249 levels (Fig. 1K, L). A strong CaLexA-GFP signal, comparable to ORNv can be observed for l2LN23
250 (LN23), a less characterized olfactory class of sparsely innervating local interneurons (Fig.1F,
251 F', M and N) (Liou et al. 2018). Fluorescence signal of Ca^{2+}-induced GFP expression quickly
252 decreases in LN23 following sensory deprivation in adult flies via removal of both antennae
253 (Fig.1O). Furthermore, an extended exposure to the ORNv inhibitor spermidine (MacWilliam
254 et al., 2018) results in a reduced CaLexA activity not only in ORNv, but also LN23, indicating a
255 preferred physiological coupling of sensory neurons to LN23 interneurons under ambient CO_2
256 conditions (Fig. 1O).

257 A predominant relay of CO_2-induced sensory activity by LN23 is supported by the modified
258 activity-dependent GRASP technique (Macpherson et al. 2015). Expression of the presynaptic
259 *syb::GFP*$^{1-10}$ in ORNv and the postsynaptic *GFP*^{11} in AL neurons revealed a significantly stronger
260 GRASP signal for ORNv→LN23 connectivity compared to the ORNv→PNv^{bi} synaptic activity
261 (Fig.2F and G). Similarly, the activity-independent tGRASP (Shearin et al. 2018) is most
262 prominent for ORNv→LN23 (Fig.2I and J), which is in line with connectome data
263 (neuPrintExplorer, hemibrain; Scheffer et al. 2020; Schlegel et al. 2021). In summary, ORNv
264 activity at ambient CO_2 levels seems to be mainly represented by the LN23 class of local
265 interneurons and less by glomerular PN relay neurons, thereby identifying a new circuit
266 component for the ORNv-induced behavioral aversion.

267

268

269

270

271 **Cell type plasticity of glomerular relay neurons following chronic CO_2 stimulation**
272

273 We next determined how the overall activity of V glomerulus relay- and interneurons changes
274 following long-lasting sensory stimulation. Adult *Drosophila melanogaster* avoids ambient
275 levels of CO_2 in a T-maze choice assay (Faucher et al. 2006; Suh et al. 2004) (Fig. 2A) but show
276 behavioral habituation following chronic CO_2 exposure (Das et al. 2011, Fig. 2B, C). The
277 reduction of CO_2-induced aversive responses is associated with an increase in the synaptic
278 volume of the V glomerulus (Fig.2D; Sachse et al. 2007 and Das et al. 2011). At the ORN level,
279 mosaic analysis revealed an extension in the surface area and size of individual synaptic
280 boutons of ORNv axons (Fig.2E). Compared to ambient CO_2 levels, prolonged elevated CO_2
281 (5%) sensation results in neuron-type specific changes of CaLexA activity (Fig. 1 H'-N')
282 (Masuyama et al. 2012). While PNv^{bi} neurons show a strong increase in Ca^{2+} levels following
283 CO_2 habituation (Fig.1I´), no CaLexA-dependent GFP expression could be observed in PNv^{uni}
284 (Fig.1J´), indicating different physiological properties of the two main glomerular CO_2 relay
285 channels (Lin et al. 2013). In addition to chronic CO_2 stimulation, short pulses of elevated CO_2
286 also did not induce Ca^{2+}-mediated-GFP expression in PNv^{uni} (Fig.1O). No significant changes in
287 CaLexA-GFP levels could be detected for LN23 neurons following prolonged CO_2 exposure
288 compared to the already high expression at ambient CO_2 conditions (Fig1M´, N´, O).

289 As GABAergic local interneurons are associated with olfactory habituation (Das et al. 2011;
290 Sadanandappa et al. 2013) we compared changes in CaLexA activation in LNv1 and LNv2 (Das
291 et al. 2011, Sachse et al. 2007). While an increase in the Ca^{2+} reporter signal could be observed
292 for both LN types following chronic CO_2 exposure, the activity of LNv1 is significantly higher
293 compared to LNv2 (Fig.1K' and L´). In line with the cell-type specific CaLexA expression,
294 previous connectome analysis showed significant differences of LN input for CO_2 relay
295 neurons: (neuPrintExplorer, hemibrain): While both PNv^{uni} and LN23 do not receive major LN-
296 type input, PNv^{bi} gains GABAergic modulation by lLN1 neurons ("bc" subtype, 16% of input)
297 and a group of multiple lLN2 neuron types (X, F, P, 19%) (Schlegel et al. 2021; Bates et al.
298 2020). These results indicate cell type specific physiological changes of glomerular neurons
299 following CO_2-induced behavioral habituation, in which PNv^{bi} shows dynamic changes in
300 glomerular connectivity while both PNv^{uni} and LN23 neurons maintained their characteristic
301 activity seen in ambient CO_2 conditions.

302 We next tested how the cell-type specific changes in neuronal activity during habituation
303 impact their synaptic connectivity within the V glomerulus. A strong increase of activity-
304 dependent sybGRASP levels for ORNv input onto PNv^{bi} could be detected following chronic
305 CO_2 stimulation (Fig.2F'). In contrast, no significant changes in sybGRASP levels were observed
306 for ORNv input onto LN23 (Fig.2G´). Of note, compared to ambient CO_2 conditions, the
307 standard deviation for ORNv→LN23 sybGRASP levels was reduced in flies chronically exposed
308 to CO_2, indicating that sensory input onto LN23 also increases in the context of habituation
309 (Fig.2H). In addition, activity-independent tGRASP expression showed that ORNs increase
310 their synaptic connections to the two main relay neurons, PNv^{bi} and LN23 (Fig.2I', J'), which is
311 in line with morphological changes of ORN axon terminals described above (Fig.2D, E).
312 Following prolonged CO_2 exposure, the PNv^{bi} class displayed increased sybGRASP levels on
313 PNv^{uni} and LN23 (Fig.2L-M'''), while no significant changes could be observed for LN23 on PNv^{bi}
314 (Fig.2N-N'''). Taken together, CO_2-induced ORNv activity seems to be relayed via two distinct
315 glomerular output channels dependent on the stimulus strength: LN23 neurons indicate
316 default ambient CO_2 levels while PNv^{bi} signals at conditions of extended elevated CO_2.

317

318 **Identity, innervation patterns and polarity of 2nd order CO_2 sensitive neurons**
319

320 To test if the difference in CaLexA activity might be related to the organization of presynaptic
321 sites within CO_2 relay neurons we visualized the active zones using *syt::GFP/brp::GFP*
322 transgenes together with the dendrite marker *DenMark::mCherry* (Kittel et al. 2006, Nicolai et
323 al. 2010; Wagh et al. 2006). PNv^{bi}, PNv^{uni} and LN23 significantly differ in their expression and
324 localization of presynaptic proteins within the dendritic compartment (Fig.3A-C). While PNv^{bi}
325 shows prominent dendritic *syt::GFP* localization throughout the glomerulus (Fig.3C), no
326 *syt::GFP* signal can be detected within PNv^{uni} dendrites (Fig.3A), indicating different cellular
327 polarity of the two main glomerular PNv classes. Despite the significant expression level,
328 *syt::GFP* appeared more scattered within LN23 dendrites and less restricted to the glomerulus
329 neuropil compared to PNv^{bi} (Fig.3B). In fact, single optical sections allow the localization of the
330 active zone marker *Brp::GFP* in LN23 dendrites outside the glomerular neuropile (Fig.3F) but
331 in PNv^{bi} confined to the V glomerulus (Fig.3G). In line with these results hemibrain EM data
332 lists enriched presynaptic site in LN23 dendrites outside the V glomerulus in contrast to the

333 restriction PNv^{bi} presynaptic sites to the glomerular neuropil (Fig.3I)
334 (https://neuprint.janelia.org/; Schlegel et al. 2021; Bates et al. 2020).

335 Following chronic sensory stimulation, PNv^{bi} showed a significant increase in the density of
336 presynaptic sites while no significant change in the amount presynaptic *syt::GFP* labeling of
337 LN23 dendrites can be observed (Fig.3D). Like the subcellular organization at ambient CO_2
338 conditions, presynaptic sites of PNv^{bi} dendrites are uniformly distributed throughout the V-
339 glomerulus (Fig.3D, last image), while most presynaptic sites of LN23 dendrites are found
340 outside of the glomerular boundaries (Fig.3D, middle image). In contrast to CO_2 relay neurons
341 PNv^{bi} and LN23, no dendritic localization of presynaptic marker transgenes could be detected
342 for PNv^{uni} (Fig.3D, first image), neither under ambient nor chronic CO_2 condition, further
343 supporting a differential synaptic profile of the two PN classes. All *syt::GFP* and
344 *DenMark::cherry* intensities were quantified using ImageJ (Fig.3H). An additional presynaptic
345 marker *syb::GFP* revealed a similar expression pattern: while PNv^{bi} showed a strong signal
346 within the glomerular boundaries, which increases following CO_2 incubation, LN23 dendrites
347 show a robust GFP signal adjacent to the neuropil border of the V glomerulus (Fig.3E). As both,
348 PNv^{bi} and PNv^{uni} are described as being excitatory, cholinergic neurons (Bates et al. 2020; Lin
349 et al. 2013; Schlegel et al. 2021; Tanaka et al. 2012) we investigated the neurotransmitter
350 identity of LN23. Anti-GABA immunostaining does not label LN23 cell bodies (Supplemental
351 Fig.3A), excluding an inhibitory function similar to canonical interglomerular LNs. These results
352 revealed not only main differences in the neuronal organization among the 3 classes of CO_2
353 relay neurons, but also a distinct response profile in intraglomerular plasticity of dendro-
354 dendritic connections. CO_2 input diverges into two more robust feed-forward channels (PNv^{uni}
355 towards LH and LN23 within the AL) while the dynamic PNv^{bi} pattern indicates intraglomerular
356 processing.

357

358 **Developmental profile of the inter-glomerular CO_2 relay neuron**
359

360 Having established the polarity of LN23, our next objective was to investigate the
361 development of this neuron, specifically focusing on how interglomerular relay neurons are
362 integrated into stereotyped antennal lobe circuits. While the glomerulus-specific assembly of
363 olfactory receptor neuron (ORN) axons with projection neuron (PN) dendrites has been

364 extensively documented (Hong & Luo 2014), less is known about the mechanisms underlying
365 the incorporation of relay neurons into these circuits. At the beginning of pupal development,
366 PN dendrites innervate the early precursor of the adult AL and occupy distinct spatial domains
367 before ORN axons enter the AL by around 20h APF (Jefferis et al. 2001; Jefferis et al. 2004).
368 LN23 neurons can be traced back to the late larval stage with a cellular morphology related to
369 SEZ (subesophageal zone) interneurons (Truman & Bate, 1988; Winding et al. 2023, Fig. 4).
370 During early pupal stages, larval LN23 precursor neurons retract from the SEZ to accumulate
371 at the ventral region of the AL precursor neuropile (Fig4A-C'). Here LN23 processes target a
372 region which is devoid of dendrites of uniglomerular PNs (Fig4F, F'). Before ORN axon arrival,
373 LN23 neurons establish a separate dendritic branch, which extends dorsally before bending
374 back to the posterior AL and merges with the main dendritic domain (Fig. 4D-E').

375 Loss of the secreted molecule *Wnt5*, which affects PN dendrite patterning (Hing et al. 2020;
376 Wu et al. 2014), leads to a continued growth of the dorsal LN23 branch along PN axon tracts
377 which exit the AL towards higher olfactory brain centers (Fig.4I-K). These results indicate that
378 LN23 neurons display an intrinsic polarity similar to uniglomerular PNs, but instead of relaying
379 sensory information from AL glomeruli to the LH/MB, a *Wnt5*-dependent mechanism seems
380 to prevent AL exit and target the presynaptic process to the extraglomerular region in the
381 ventral AL. In wild type, ORN axons innervate the developing V glomerulus only at the
382 ipsilateral AL, in contrast to the majority of bilateral ORN classes (Fig.4F-H) (Couto et al. 2005).
383 To gain insight into the mechanisms which support glomerulus-specific ORNv input on LN23,
384 we analyzed candidate genes which are expressed on growing ORNs. Mutations in the
385 protocadherin-type cell adhesion molecule Flamingo (*fmi*), which is highly enriched on ORN
386 axons in the developing V glomerulus, affect their synaptic targeting. Here, *fmi* mutant ORNv
387 axons are no longer restricted to the glomerular boundaries but extend into the posterior AL
388 next to the output domain of LN23 (Suppl.Fig.4A, B), indicating cellular interactions to restrict
389 class-specific axon-dendrite recognition within the glomerular domain.

390 In summary, despite being morphologically classified as a local interneuron, the LN23 class
391 shows cellular and developmental features related to olfactory projection neurons: a highly
392 polarized neuronal morphology in the adult olfactory system is established by a glomerulus-
393 specific dendrite targeting for singular ORN input and a default axonal extension along
394 olfactory PN tracts rerouted by external signals (Komiyama & Luo, 2006).

395 **LN23 mediates CO_2-induced aversion**
396

397 To test the role of the different CO_2 relay neurons on Drosophila behavior, we expressed the
398 shibire^{ts} transgene to block synaptic transmission in a cell type specific manner (Chen et al.
399 1991; Kitamoto 2001). Neuronal silencing of each of the two glomerular PNs led to a reduction
400 of the innate CO_2 avoidance, with stronger effects observed for PNv^{uni} compared to PNv^{bi} (Fig.
401 5A). While CO_2 avoidance can still be observed following the neuronal silencing of each PN
402 class, shibire^{ts} induced silencing of LN23 fully abolished aversion behavior towards CO_2 (Fig.
403 5A). To test for cell type specificity of the behavioral phenotype following LN23 silencing, we
404 used the Ca^{2+} dependent LexA activation of the CaLexA construct for shi^{ts} expression and
405 observed a reduction of the innate CO_2 aversion (Fig. 5B) (Masuyama et al. 2012). To increase
406 lexA levels we chronically exposed flies to high levels of CO_2. Interestingly, increased CaLexA
407 mediated shi^{ts} expression via chronic exposure not only suppressed behavioral aversion but
408 led to a significant level of attraction towards CO_2 (Fig.5B). These results indicate a prominent
409 function of LN23 in CO_2 valence coding: Blocking LN23 activity is sufficient to fully suppress
410 CO_2 behavioral aversion and together with the GABAergic suppression of PNv^{bi} during
411 habituation an attraction towards CO_2 is observed, which phenocopies the silencing of ORNv
412 (Jones et al. 2007; Kwon et al. 2007, MacWilliam et al. 2018; Suh et al. 2004).

413 To further determine if these relay neurons are sufficient for behavioral aversion, we
414 optogenetically activated each neuron type and measured the behavioral response (Inagaki
415 et al. 2014; Klapoetke et al. 2014; Pulver et al. 2009) (see M&M). Light-induced activation of
416 ORNv (*GR21a-Gal4*) expressing UAS-ReaCh led to strong aversion (Fig. 5C). Similarly,
417 optogenetically activated LN23 is sufficient to trigger behavioral aversion via two independent
418 Gal4 driver lines (LN23 Gal4 and the alternative line we used: VT48408-Gal4; Fig.5C) or by $Ca2^{+}$
419 induced LexA activation (Fig.5D). In contrast, no change in light-induced activation for both,
420 PNv^{bi} (two independent driver lines, see Methods) nor PNv^{uni} could be observed (Fig.5C).
421 These results support a predominant role of LN23 in CO_2-induced avoidance behavior.
422 Compared to the more dynamic activity of PNv^{bi} following acute and chronic sensory
423 stimulation, LN23 shows little changes in intrinsic activity, representing ORNv activity
424 independent of changes in CO_2 levels or temporal pattern. Based on these findings we propose
425 a ground state of ORNv/LN23 mediated aversion induced by ambient CO_2 default state, which
426 is modified either by the parallel PN channels or downstream of LN23.

427 **3rd order neurons postsynaptic to LN23 have a putative role in valence coding**
428

429 To gain further insights into the unique organization of the LN23 pathway compared to the
430 glomerular relay channel, we analyzed the postsynaptic candidate neurons within the
431 posterior AL. Two PN types, l2_PNm17 and sm_PNm1 are receiving a large proportion of their
432 synaptic input (27% and 18%, respectively) from LN23 (Fig.6A, neuPrint, Janelia Research
433 Campus; https://neuprint.janelia.org/; Schlegel et al. 2021). Like the two PN classes of the V
434 glomerulus, PNm1 and PNm17 show distinct relay properties: While input into PNm1 is mostly
435 restricted to the LN23-CO_2 channel, dendrites of PNm17 extend into adjacent VP1 and VP3-5
436 glomeruli to receive direct input from thermo- and humidity- receptor neurons (neuPrint,
437 Janelia Research Campus; https://neuprint.janelia.org/; Frank et al. 2015; Marin et al. 2020).
438 Both types of non-olfactory relay neurons target multiple distinct brain areas adjacent to the
439 canonical olfactory LH, the posterior lateral protocerebrum (PLP), superior clamp (SCL) and
440 the superior lateral protocerebrum (SLP) (Fig6 A, B, C) (Ito et al. 2014). To visualize the
441 trajectories of the PNs, we used MCFO (Aso et al. 2014) to create single cell clones, which
442 show that PNm1 and PNm17 axons turn close before entering the LH to target adjacent brain
443 regions (Fig. 6B, C). Of note, compared to glomerular PNv^{uni} and PNv^{bi}, PNm1 and PNm17
444 receive only minor input from GABAergic LNs (neuPrint, Janelia Research Campus;
445 https://neuprint.janelia.org/), indicating reduced gain control properties of the extra-
446 glomerular ORN→LN23→PNm pathway (Olsen & Wilson, 2008).

447 Optogenetic activation of each of the two PNm class neurons downstream of LN23 induce
448 opposite behavioral responses: While activity of the "CO_2-only" class PNm1 results in strong
449 aversion, the "multi-modal" PNm17 initiates behavioral attraction (Fig.6D). Furthermore, CO_2-
450 induced aversive behavior could be attenuated following shi^{ts}-mediated silencing of PNm1 but
451 was not changed by silencing PNm17 (Fig.6 E, F). Interestingly, FlyWire.ai (Dorkenwald et al.
452 2024; Eckstein et al. 2024; Schlegel et al. 2024; Zheng et al. 2018) revealed distinct
453 neurotransmitter identities for the two PNm classes, GABA expression for PNm1, while PNm17
454 is showing a cholinergic synaptic profile. Together with the behavioral responses following
455 optogenetic activation this suggests a circuit motif in which the default activity of the
456 ORNv→LN23→PNm1 channel by ambient CO_2 sensation blocks a central brain region
457 important for behavioral attraction (Dolan et al. 2019).

458

459 **Connectivity in higher brain centers and lateral communication in the antennal lobe**
460

461 As the glomerular PNs and the extra-glomerular LN23→PNm channels target adjacent central
462 brain regions we were wondering if the two parallel CO_2 pathways converge onto common
463 downstream neurons. The hemibrain dataset (https://neuprint.janelia.org/; Plaza et al. 2022;
464 Scheffer et al. 2020) identified three main types of glutamatergic LH neurons (FlyWire.ai;
465 Dorkenwald et al. 2024; Eckstein et al. 2024; Schlegel et al. 2024; Zheng et al. 2018) as PNv or
466 PNm targets: LH^{PD5c1} as the primary target of PNv^{bi} (Fig.6 G), LH^{PV9b1} downstream of PNm1
467 (Fig.6 H) and LH^{CENT4} as the major postsynaptic partner of PNv^{uni} (Fig.6 I). All 3 LH target
468 neurons of the parallel CO_2 pathways are directly interconnected (Fig. 8): While LH^{PV9b1} not
469 only receives input from PNm1 but also from PNv^{bi}, LH^{PD5c1}, the main downstream target of
470 PNv^{bi}, is also targeted by LH^{CENT4}, the primary postsynaptic partner of PNv^{uni}. This core motif
471 of CO_2 perception receives additional input from other sensory modalities. LH^{PD5c1} gains input
472 from "food-sensing" glomeruli (DM4, DC4/DP1, and VM7) via class-specific cholinergic PNs,
473 indicating a neuronal integrator of CO_2 and food-related cues (Couto et al. 2005; Dumenil et
474 al. 2025; Min et al. 2013). In addition, LH^{CENT4} is also a main target for $l2PN^{VP4+VL1}$, mediating
475 the perception of dryness and pyrrolidine-type odorants, thereby adding another layer of
476 multimodal sampling to the LN23 → PNm1 pathway (Fig.8) (Li et al. 2022; Choi et al. 2022; Ni
477 2021). Interestingly, the convergence of the glomerular CO_2 and food channels is not only
478 observed for LH neurons downstream of AL relay pathways but seems to occur already at the
479 level of AL glomeruli. Hemibrain describes with l2LN19 another class of polarized local
480 interneuron (Fig.7A, B) with enriched postsynaptic sites at "food-sensing" glomeruli DM4,
481 DC4/DP1, and VM7 (Fig.7A) as well as targeted output onto PNv^{bi} and PNv^{uni} in the V-
482 glomerulus (Fig.7B), but merely with LN23 (Fig.7C) (https://neuprint.janelia.org/; Schlegel et
483 al. 2021; Bates et al.2020). Accordingly, optogenetic activation of LN19 led to an aversive
484 behavioral response (Fig.7D), while inhibition had no effect (Fig.7E).

485 Based on these distinct connectivity patterns and behavioral response profiles of individual
486 relay neurons we are proposing the following circuit mechanism for CO_2 valence coding (Fig.8):
487 The activity of CO_2-responsive sensory neurons (ORNv, black) is relayed by parallel PN
488 channels and converge onto two central brain target neurons of opposite intrinsic valence
489 identity. The glomerular PNs target the ventral domain of LH^{PD5} to trigger behavioral aversion
490 and extraglomerular PNs activated via the lateral LN23 relay converge onto LH^{PV9} which

491 mediates attraction. While PNm17 supports LH^{PV9} activity, GABAergic PNm1 blocks LH^{PV9}
492 through which the negative valence state of LH^{PD5} triggers avoidance. This core aversion
493 pathway (PNv^{bi}/PNv^{uni}/PNm1), without prominent GABAergic modulation, directly represents
494 the activity of CO_2 sensory neurons, is modified either via the activation of the dorsal LH^{PD5}
495 domain by fruit odor PNs ($PN^{DM/VM/DC}$) or by an increase of PNm17 through non-olfactory
496 sensory neurons to support a context-dependent behavioral response repertoire.

497 **Discussion**
498

499 In Drosophila, the activation of a single class of CO_2 receptive sensory neurons induces
500 avoidance behavior, which is modified by multiple external and internal stimuli (Bräcker et al.
501 2013; Faucher et al. 2006; Dissegna et al. 2021; Suh et al. 2004; Turner and Ray, 2009). How
502 does the Drosophila brain transforms ORNv input into flexible behavioral responses towards
503 CO_2? Here we identified a novel CO_2 relay channel with unique morphological and
504 physiological properties compared to the canonical glomerular PN pathway. First, instead of
505 direct transmission of sensory input by glomerular PNs in the anterior AL towards higher brain
506 centers, the ORNv induced activation of the local interneuron LN23 relays peripheral CO_2
507 sensation to an extraglomerular neuropil of the posterior AL generating two parallel output
508 channels with different target areas. Second, in contrast to the high level of neuronal plasticity
509 observed for PNs within glomerular circuits, LN23 analysis revealed very little dynamic
510 changes under different physiological conditions. This might be due to distinct intrinsic
511 features of PNs and LN23 such as the expression of ion channels or receptor molecules but
512 could also be explained by the absence of glomerular GABAergic neurons at the
513 extraglomerular CO_2 pathway. Third, following the manipulation of neuronal activity, only
514 LN23, but no individual PNs are able to induce an aversive behavioral response similar to
515 ORNv. Finally, the extraglomerular CO_2 pathway includes a structural segregation of opposite
516 valence-encoding elements, in which the "CO_2-only" neuron induces aversion while activation
517 of the parallel "multi-modal" channel determines behavioral attraction. These findings are
518 consistent with a designated circuit motif encoding a default behavioral state of avoidance
519 even under atmospheric CO_2 levels. As the "CO_2-only" relay neuron PNm1 has a predicted
520 GABAergic identity (FlyWire.ai; Dorkenwald et al. 2024; Eckstein et al. 2024; Schlegel et al.
521 2024; Zheng et al. 2018), the previously reported ORNv induced avoidance (MacWilliam et al.

522 2018; Das et al. 2011) could be explained with the inhibition of a premotor area by the LN23
523 channel.

524 The interplay between the extraglomerular default channel and the glomerular dynamic
525 pathway in encoding behavioral avoidance was demonstrated in the context of habituation.
526 While the increased GABAergic inhibition of glomerular PNs following chronic CO_2 sensation
527 reduces innate aversion, the simultaneous silencing of LN23 not only eliminates all aversive
528 response features but reverses CO_2 valence to trigger attraction. Interestingly, the reduced
529 aversion through inhibition of PN activity in the context of habituation seems partially
530 compensated by increasing PNv^{bi} synaptic plasticity. We observed a strong gain of presynaptic
531 sites of glomerular PNv^{bi} dendrites onto LN23, which might maintain a balanced level of
532 aversion activity for local CO_2 levels following habitation (Das et al. 2011; Sachse et al. 2007).
533 Although both PNv^{uni} and PNv^{bi} are excitatory cholinergic projection neurons (Tanaka et al.
534 2012; Lin et al. 2013; Bates et al. 2020; Schlegel et al. 2021), they differ in their cellular
535 organization and behavioral function. In contrast to PNv^{bi}, PNv^{uni} dendrites lack presynaptic
536 sites, therefore specifies a feed-forward channel similar to LN23. Based on these results we
537 are proposing complementary function of the three relay neurons in mediating flexible CO_2
538 behavioral response patterns: While LN23 encodes default avoidance under ambient
539 conditions, supported by PNv^{uni} as a sensor for elevated local levels of CO_2, PNv^{bi} defines the
540 main component of experience-dependent modulation by LNs and neurons of the MB calyx
541 (CA) (Bräcker et al. 2013).

542 Interestingly, developmental analysis revealed a polarized growth pattern of LN23 that
543 resembles projection neurons more than typical local interneurons (Jefferis et al. 2004;
544 Komiyama & Luo 2006). LN23 originates from a larval interneuron located in the
545 suboesophageal zone (SEZ), which undergoes remodeling into an adult olfactory interneuron
546 during early pupal stages (Truman & Bate, 1988). We hypothesize that the secreted *Wnt5*
547 protein, a critical factor for initial projection neuron dendrite patterning, supports the
548 targeting of LN23 processes to the posterior antennal lobe (AL) region. Like the genetically
549 defined recognition mechanisms that guide glomerulus-specific ORN-PN connectivity, growing
550 ORNv axons appear to target LN23 dendrites as synaptic partners. Since LN23 dendrites are
551 organized into a defined glomerular input and extraglomerular output zone, we propose

552 Flamingo-dependent expression on ingrowing ORN axons to prevent sensory input to LN23
553 outside the glomerular domain.

554 The divergence of CO_2-induced ORN activation into parallel relay channels allows for early
555 convergence of additional sensory information. This includes not only the integration of non-
556 olfactory cues by the positive valence branch PNm17 downstream of LN23 (Frank et al. 2015;
557 Li et al. 2022), but also the sampling of food-odor-sensitive glomeruli by the polarized
558 interneuron LN19 for V-glomerulus input (Couto et al. 2005; Dumenil et al. 2025; Min et al.
559 2013). The convergence of different parallel CO_2 channels onto a common set of lateral horn
560 (LH) interneurons suggests a potential hub for motor action control (Dolan et al. 2019). The
561 results presented in this study support a conceptual model in which the default state of
562 behavioral aversion, induced through inhibition of an LH motor hub by the "CO_2-only"
563 ORNv→LN23→PNm1 pathway, is modified by the inclusion of additional glomerular and
564 extraglomerular projection neuron classes to allow approach behavior. Further studies on the
565 physiological architecture of the CO_2 core circuit within and downstream of the LH may reveal
566 deeper insights into the multimodal processing underlying flexible, context-dependent
567 behaviors.

568 Additionally, despite the conserved molecular receptor identity of CO_2 sensory neurons
569 among insects, species-specific behavioral responses to local CO_2 concentrations are evident
570 (Turner & Ray 2009). In many species, such as mosquitoes, elevated CO_2 levels signal potential
571 food sources and elicit attraction (Tauxe et al. 2013; Siju 2009; Ghaninia 2007). The
572 identification of a dedicated CO_2 aversion channel in *D. melanogaster* opens new avenues for
573 comparative research into circuit motifs and offers insight into the neural basis of behavioral
574 flexibility across insect evolution (Oram & Card 2022).

575

576

577

578

579

580 **References**

581

582 **Aso, Y., Hattori, D., Yu, Y., Johnston, R. M., Iyer, N. A., Ngo, T. T., Dionne, H., Abbott, L. F.,**
583 **Axel, R., Tanimoto, H., & Rubin, G. M. (2014).** The neuronal architecture of the mushroom
584 body provides a logic for associative learning. *eLife*, *3*, e04577.
585 https://doi.org/10.7554/eLife.04577

586 **Bates, A. S., Schlegel, P., Roberts, R. J. V., Drummond, N., Tamimi, I. F. M., Turnbull, R., Zhao,**
587 **X., Marin, E. C., Popovici, P. D., Dhawan, S., Jamasb, A., Javier, A., Serratosa Capdevila, L., Li,**
588 **F., Rubin, G. M., Waddell, S., Bock, D. D., Costa, M., & Jefferis, G. S. X. E. (2020).** Complete
589 Connectomic Reconstruction of Olfactory Projection Neurons in the Fly Brain. *Current biology*
590 *: CB*, *30*(16), 3183–3199.e6. https://doi.org/10.1016/j.cub.2020.06.042

591 **Bräcker, L. B., Siju, K. P., Varela, N., Aso, Y., Zhang, M., Hein, I., Vasconcelos, M. L., &**
592 **Grunwald Kadow, I. C. (2013).** Essential role of the mushroom body in context-dependent CO_2
593 avoidance in Drosophila. *Current biology : CB*, *23*(13), 1228–1234.
594 https://doi.org/10.1016/j.cub.2013.05.029

595 **Das Chakraborty, S., Chang, H., Hansson, B. S., & Sachse, S. (2022).** Higher-order olfactory
596 neurons in the lateral horn support odor valence and odor identity coding
597 in *Drosophila*. *eLife*, *11*, e74637. https://doi.org/10.7554/eLife.74637

598 **Chen, M. S., Obar, R. A., Schroeder, C. C., Austin, T. W., Poodry, C. A., Wadsworth, S. C., &**
599 **Vallee, R. B. (1991).** Multiple forms of dynamin are encoded by shibire, a Drosophila gene
600 involved in endocytosis. *Nature*, *351*(6327), 583–586. https://doi.org/10.1038/351583a0

601 **Choi, K., Kim, W. K., & Hyeon, C. (2022).** Olfactory responses of *Drosophila* are encoded in the
602 organization of projection neurons. *eLife*, *11*, e77748. https://doi.org/10.7554/eLife.77748

603 **Couto, A., Alenius, M., & Dickson, B. J. (2005).** Molecular, anatomical, and functional
604 organization of the Drosophila olfactory system. *Current biology : CB*, *15*(17), 1535–1547.
605 https://doi.org/10.1016/j.cub.2005.07.034

606

607

Das, S., Sadanandappa, M. K., Dervan, A., Larkin, A., Lee, J. A., Sudhakaran, I. P., Priya, R., Heidari, R., Holohan, E. E., Pimentel, A., Gandhi, A., Ito, K., Sanyal, S., Wang, J. W., Rodrigues, V., & Ramaswami, M. (2011). Plasticity of local GABAergic interneurons drives olfactory habituation. *Proceedings of the National Academy of Sciences of the United States of America*, *108*(36), E646–E654. https://doi.org/10.1073/pnas.1106411108

Dissegna, A., Turatto, M., & Chiandetti, C. (2021). Context-Specific Habituation: A Review. *Animals : an open access journal from MDPI*, *11*(6), 1767. https://doi.org/10.3390/ani11061767

Dolan, M. J., Frechter, S., Bates, A. S., Dan, C., Huoviala, P., Roberts, R. J. V., Schlegel, P., Dhawan, S., Tabano, R., Dionne, H., Christoforou, C., Close, K., Sutcliffe, B., Giuliani, B., Feng, L., Costa, M., Ihrke, G., Meissner, G. W., Bock, D. D., Aso, Y., Rubin, G. M., & Jefferis, G. S. X. E. (2019). Neurogenetic dissection of the Drosophila lateral horn reveals major outputs, diverse behavioural functions, and interactions with the mushroom body. *eLife, 8*, e43079. https://doi.org/10.7554/eLife.43079

Dorkenwald, S., Matsliah, A., Sterling, A. R., Schlegel, P., Yu, S. C., McKellar, C. E., Lin, A., Costa, M., Eichler, K., Yin, Y., Silversmith, W., Schneider-Mizell, C., Jordan, C. S., Brittain, D., Halageri, A., Kuehner, K., Ogedengbe, O., Morey, R., Gager, J., Kruk, K., … FlyWire Consortium (2024). Neuronal wiring diagram of an adult brain. *Nature*, *634*(8032), 124–138. https://doi.org/10.1038/s41586-024-07558-y

Dumenil, C., Yildirim, G., & Haase, A. (2025). Differential Coding of Fruit, Leaf, and Microbial Odours in the Brains of *Drosophila suzukii* and *Drosophila melanogaster*. *Insects*, *16*(1), 84. https://doi.org/10.3390/insects16010084

Eckstein, N., Bates, A. S., Champion, A., Du, M., Yin, Y., Schlegel, P., Lu, A. K., Rymer, T., Finley-May, S., Paterson, T., Parekh, R., Dorkenwald, S., Matsliah, A., Yu, S. C., McKellar, C., Sterling, A., Eichler, K., Costa, M., Seung, S., Murthy, M., … Funke, J. (2024). Neurotransmitter classification from electron microscopy images at synaptic sites in Drosophila melanogaster. *Cell*, *187*(10), 2574–2594.e23. https://doi.org/10.1016/j.cell.2024.03.016

Faucher, C., Forstreuter, M., Hilker, M., & de Bruyne, M. (2006). Behavioral responses of Drosophila to biogenic levels of carbon dioxide depend on life-stage, sex and olfactory context. *The Journal of experimental biology*, *209*(Pt 14), 2739–2748. https://doi.org/10.1242/jeb.02297

Frank, D. D., Jouandet, G. C., Kearney, P. J., Macpherson, L. J., & Gallio, M. (2015). Temperature representation in the Drosophila brain. *Nature*, *519*(7543), 358–361. https://doi.org/10.1038/nature14284

Frechter, S., Bates, A. S., Tootoonian, S., Dolan, M. J., Manton, J., Jamasb, A. R., Kohl, J., Bock, D. D., & Jefferis, G. S. X. E. (2019). Functional and anatomical specificity in a higher olfactory centre. *eLife*, 8, e44590. https://doi.org/10.7554/eLife.44590

Ghaninia, M. (2007). *Olfaction in Mosquitoes.* Doctoral Thesis, Swedish University of Agricultural Sciences. https://pub.epsilon.slu.se/1560/.

Grabe, V., Baschwitz, A., Dweck, H. K. M., Lavista-Llanos, S., Hansson, B. S., & Sachse, S. (2016). Elucidating the neuronal architecture of olfactory glomeruli in the Drosophila antennal lobe. *Cell Reports*, 16(12), 3401–3413. https://doi.org/10.1016/j.celrep.2016.08.063

Hansson, B. S., & Stensmyr, M. C. (2011). Evolution of insect olfaction. *Neuron, 72*(5), 698–711. https://doi.org/10.1016/j.neuron.2011.11.003

Hing, H., Reger, N., Snyder, J., & Fradkin, L. G. (2020). Interplay between axonal Wnt5-Vang and dendritic Wnt5-Drl/Ryk signaling controls glomerular patterning in the Drosophila antennal lobe. *PLoS genetics*, *16*(5), e1008767. https://doi.org/10.1371/journal.pgen.1008767

Hong, W., & Luo, L. (2014). Genetic control of wiring specificity in the fly olfactory system. *Genetics*, 196(1), 17–29. https://doi.org/10.1534/genetics.113.154336

Inagaki, H. K., Jung, Y., Hoopfer, E. D., Wong, A. M., Mishra, N., Lin, J. Y., Tsien, R. Y., & Anderson,D.J.(2014). Optogenetic control of *Drosophila* using a red-shifted channelrhodopsin (ReaChR). *Nature Methods, 11*(3), 325–332. https://doi.org/10.1038/nmeth.2765

Ito, K., Shinomiya, K., Ito, M., Armstrong, J. D., Boyan, G., Hartenstein, V., Harzsch, S., Heisenberg, M., Homberg, U., Jenett, A., Keshishian, H., Restifo, L. L., Rössler, W., Simpson, J. H., Strausfeld, N. J., Strauss, R., Vosshall, L. B., & Insect Brain Name Working Group (2014). A systematic nomenclature for the insect brain. *Neuron*, *81*(4), 755–765. https://doi.org/10.1016/j.neuron.2013.12.017

Jefferis, G. S., Marin, E. C., Stocker, R. F., & Luo, L. (2001). Target neuron prespecification in the olfactory map of Drosophila. *Nature*, *414*(6860), 204–208. https://doi.org/10.1038/35102574

Jefferis, G. S., Vyas, R. M., Berdnik, D., Ramaekers, A., Stocker, R. F., Tanaka, N. K., Ito, K., & Luo, L. (2004). Developmental origin of wiring specificity in the olfactory system of Drosophila. *Development (Cambridge, England)*, *131*(1), 117–130. https://doi.org/10.1242/dev.00896

Jones, W. D., Cayirlioglu, P., Kadow, I. G., & Vosshall, L. B. (2007). Two chemosensory receptors together mediate carbon dioxide detection in *Drosophila*. *Nature*, 445(7123), 86–90. https://doi.org/10.1038/nature05466

Kitamoto T. (2001). Conditional modification of behavior in Drosophila by targeted expression of a temperature-sensitive shibire allele in defined neurons. *Journal of neurobiology*, *47*(2), 81–92. https://doi.org/10.1002/neu.1018

Kittel, R. J., Wichmann, C., Rasse, T. M., Fouquet, W., Schmidt, M., Schmid, A., Wagh, D. A., Pawlu, C., Kellner, R. R., Willig, K. I., Hell, S. W., Buchner, E., Heckmann, M., & Sigrist, S. J. (2006). Bruchpilot promotes active zone assembly, Ca2+ channel clustering, and vesicle release. *Science (New York, N.Y.)*, *312*(5776), 1051–1054. https://doi.org/10.1126/science.1126308

Klapoetke, N. C., Murata, Y., Kim, S. S., Pulver, S. R., Birdsey-Benson, A., Cho, Y. K., Morimoto, T. K., Chuong, A. S., Carpenter, E. J., Tian, Z., Wang, J., Xie, Y., Yan, Z., Zhang, Y., Chow, B. Y., Surek, B., Melkonian, M., Jayaraman, V., Constantine-Paton, M., Wong, G. K., … Boyden, E. S. (2014). Independent optical excitation of distinct neural populations. *Nature methods*, *11*(3), 338–346. https://doi.org/10.1038/nmeth.2836

692 **Komiyama, T., & Luo, L. (2006).** Development of wiring specificity in the olfactory
693 system. *Current opinion in neurobiology*, *16*(1), 67–73.
694 https://doi.org/10.1016/j.conb.2005.12.002

695 **Koyama, T., Rodrigues, M. A., Athanasiadis, A., Shingleton, A. W., & Mirth, C. K. (2021).**
696 A nutrient-responsive hormonal circuit mediates an inter-organ growth coordination in
697 *Drosophila*.*Nature Communications, 12*, 7168.
698 https://doi.org/10.1038/s41467-021-25445-2

699 **Kwon, J. Y., A. Dahanukar, L. A. Weiss, and J. R. Carlson. (2007).** The Molecular Basis of CO_2
700 Reception in Drosophila. *Proceedings of the National Academy of Sciences USA* 104 (9): 3574–
701 78. https://doi.org/10.1073/pnas.0700079104.

702 **Lewis, L. P. C., Siju, K. P., Aso, Y., Friedrich, A. B., Bulteel, A. J. B., Rubin, G. M., & Grunwald**
703 **Kadow, I. C. (2015).** A higher brain circuit for immediate integration of conflicting sensory
704 information in *Drosophila*. *Current Biology, 25*(17), 2203–2214.
705 https://doi.org/10.1016/j.cub.2015.07.015

706 **Li, S., Li, B., Gao, L., Wang, J., & Yan, Z. (2022).** Humidity response in Drosophila olfactory
707 sensory neurons requires the mechanosensitive channel TMEM63. *Nature*
708 *communications*, *13*(1), 3814. https://doi.org/10.1038/s41467-022-31253-z

709 **Lin, H. H., Chu, L. A., Fu, T. F., Dickson, B. J., & Chiang, A. S. (2013).** Parallel neural pathways
710 mediate CO_2 avoidance responses in Drosophila. *Science (New York, N.Y.)*, *340*(6138), 1338–
711 1341. https://doi.org/10.1126/science.1236693

712 **Liou, N. F., Lin, S. H., Chen, Y. J., Tsai, K. T., Yang, C. J., Lin, T. Y., Wu, T. H., Lin, H. J., Chen, Y.**
713 **T., Gohl, D. M., Silies, M., & Chou, Y. H. (2018).** Diverse populations of local interneurons
714 integrate into the Drosophila adult olfactory circuit. *Nature communications*, *9*(1), 2232.
715 https://doi.org/10.1038/s41467-018-04675-x

716 **Macpherson, L. J., Zaharieva, E. E., Kearney, P. J., Alpert, M. H., Lin, T. Y., Turan, Z., Lee, C.**
717 **H., & Gallio, M. (2015).** Dynamic labelling of neural connections in multiple colours by trans-
718 synaptic fluorescence complementation. *Nature communications*, *6*, 10024.
719 https://doi.org/10.1038/ncomms10024

720 **MacWilliam, D., J. Kowalewski, A. Kumar, C. Pontrello, and A. Ray. (2018).** Signaling Mode of
721 the Broad-Spectrum Conserved CO_2 Receptor Is One of the Important Determinants of Odor
722 Valence in Drosophila. *Neuron* 97 (5): 1153–67.e4.
723 https://doi.org/10.1016/j.neuron.2018.01.028.

724 **Marin, E. C., Büld, L., Theiss, M., Sarkissian, T., Roberts, R. J. V., Turnbull, R., Tamimi, I. F. M.,**
725 **Pleijzier, M. W., Laursen, W. J., Drummond, N., Schlegel, P., Bates, A. S., Li, F., Landgraf, M.,**
726 **Costa, M., Bock, D. D., Garrity, P. A., & Jefferis, G. S. X. E. (2020).** Connectomics Analysis
727 Reveals First-, Second-, and Third-Order Thermosensory and Hygrosensory Neurons in the
728 Adult Drosophila Brain. *Current biology : CB*, *30*(16), 3167–3182.e4.
729 https://doi.org/10.1016/j.cub.2020.06.028

730 **Masuyama, K., Zhang, Y., Rao, Y., & Wang, J. W. (2012).** Mapping neural circuits with activity-
731 dependent nuclear import of a transcription factor. *Journal of neurogenetics*, *26*(1), 89–102.
732 https://doi.org/10.3109/01677063.2011.642910

733 **Min, S., Ai, M., Shin, S. A., & Suh, G. S. (2013).** Dedicated olfactory neurons mediating
734 attraction behavior to ammonia and amines in Drosophila. *Proceedings of the National*
735 *Academy of Sciences of the United States of America*, *110*(14), E1321–E1329.
736 https://doi.org/10.1073/pnas.1215680110

737 **Nagel, K. I., & Wilson, R. I. (2016).** Mechanisms underlying population response dynamics in
738 inhibitory interneurons of the *Drosophila* antennal lobe. *Journal of Neuroscience, 36*(14),
739 4325–4338. https://doi.org/10.1523/JNEUROSCI.3887-15.2016

740 **Nern, A., Pfeiffer, B. D., & Rubin, G. M. (2015).** Optimized tools for multicolor stochastic
741 labeling reveal diverse stereotyped cell arrangements in the fly visual system. *PNAS*, 112(22),
742 E2967–E2976. https://doi.org/10.1073/pnas.1506763112

743 **Ni L. (2021).** The Structure and Function of Ionotropic Receptors in *Drosophila*. *Frontiers in*
744 *molecular neuroscience*, *13*, 638839. https://doi.org/10.3389/fnmol.2020.638839

745 **Nicolaï, L. J., Ramaekers, A., Raemaekers, T., Drozdzecki, A., Mauss, A. S., Yan, J., Landgraf,**
746 **M., Annaert, W., & Hassan, B. A. (2010).** Genetically encoded dendritic marker sheds light on
747 neuronal connectivity in Drosophila. *Proceedings of the National Academy of Sciences of the*
748 *United States of America*, *107*(47), 20553–20558. https://doi.org/10.1073/pnas.1010198107

Olsen, S. R., & Wilson, R. I. (2008). Lateral presynaptic inhibition mediates gain control in an olfactory circuit. *Nature*, *452*(7190), 956–960. https://doi.org/10.1038/nature06864

Oram, T. B., & Card, G. M. (2022). Context-dependent control of behavior in Drosophila. *Current opinion in neurobiology*, *73*, 102523. https://doi.org/10.1016/j.conb.2022.02.003

Plaza, S. M., Clements, J., Dolafi, T., Umayam, L., Neubarth, N. N., Scheffer, L. K., & Berg, S. (2022). *neu*Print: An open access tool for EM connectomics. *Frontiers in neuroinformatics*, *16*, 896292. https://doi.org/10.3389/fninf.2022.896292

Pulver, S. R., Pashkovski, S. L., Hornstein, N. J., Garrity, P. A., & Griffith, L. C. (2009). Temporal dynamics of neuronal activation by Channelrhodopsin-2 and TRPA1 determine behavioral output in *Drosophila* larvae. *Journal of Neurophysiology, 101*(6), 3075–3088. https://doi.org/10.1152/jn.00071.2009

Root, C. M., Masuyama, K., Green, D. S., Enell, L. E., Nässel, D. R., Lee, C. H., & Wang, J. W. (2008). A presynaptic gain control mechanism fine-tunes olfactory behavior. *Neuron*, *59*(2), 311–321. https://doi.org/10.1016/j.neuron.2008.07.003

Sachse, S., & Beshel, J. (2016). The good, the bad, and the hungry: how the central brain codes odor valence to facilitate food approach in Drosophila. *Current opinion in neurobiology*, *40*, 53–58. https://doi.org/10.1016/j.conb.2016.06.012

Sachse, S., Rueckert, E., Keller, A., Okada, R., Tanaka, N. K., Ito, K., & Vosshall, L. B. (2007). Activity-dependent plasticity in an olfactory circuit. *Neuron*, *56*(5), 838–850. https://doi.org/10.1016/j.neuron.2007.10.035

Sadanandappa, M. K., Redondo, B. B., Michels, B., Rodrigues, V., Gerber, B., VijayRaghavan, K., Buchner, E., & Ramaswami, M. (2013). Synapsin function in GABA-ergic interneurons is required for short-term olfactory habituation. *Journal of Neuroscience, 33*(42), 16576–16585. https://doi.org/10.1523/JNEUROSCI.3142-13.2013

Scheffer, L. K., Xu, C. S., Januszewski, M., Lu, Z., Takemura, S. Y., Hayworth, K. J., Huang, G. B., Shinomiya, K., Maitlin-Shepard, J., Berg, S., Clements, J., Hubbard, P. M., Katz, W. T., Umayam, L., Zhao, T., Ackerman, D., Blakely, T., Bogovic, J., … Meinertzhagen, I. A. (2020). A connectome and analysis of the adult Drosophila central brain. *eLife, 9*, e57443. https://doi.org/10.7554/eLife.57443

Schlegel, P., Bates, A. S., Stürner, T., Jagannathan, S. R., Drummond, N., Hsu, J., Serratosa Capdevila, L., Javier, A., Marin, E. C., Barth-Maron, A., Tamimi, I. F., Li, F., Rubin, G. M., Plaza, S. M., Costa, M., & Jefferis, G. S. X. E. (2021). Information flow, cell types and stereotypy in a full olfactory connectome. *eLife*, *10*, e66018. https://doi.org/10.7554/eLife.66018

Schlegel, P., Yin, Y., Bates, A. S., Dorkenwald, S., Eichler, K., Brooks, P., Han, D. S., Gkantia, M., Dos Santos, M., Munnelly, E. J., Badalamente, G., Serratosa Capdevila, L., Sane, V. A., Fragniere, A. M. C., Kiassat, L., Pleijzier, M. W., Stürner, T., Tamimi, I. F. M., Dunne, C. R., Salgarella, I., … Jefferis, G. S. X. E. (2024). Whole-brain annotation and multi-connectome cell typing of Drosophila. *Nature*, *634*(8032), 139–152. https://doi.org/10.1038/s41586-024-07686-5

Semelidou, O., Acevedo, S. F., & Skoulakis, E. M. (2018). Temporally specific engagement of distinct neuronal circuits regulating olfactory habituation in *Drosophila*. *eLife*, *7*, e39569. https://doi.org/10.7554/eLife.39569

Shearin, H. K., Quinn, C. D., Mackin, R. D., Macdonald, I. S., & Stowers, R. S. (2018). t-GRASP, a targeted GRASP for assessing neuronal connectivity. *Journal of neuroscience methods*, *306*, 94–102. https://doi.org/10.1016/j.jneumeth.2018.05.014

Siju, K. P. (2009). *Neuromodulation in the Chemosensory System of Mosquitoes: Neuroanatomy and Physiology.* Doctoral Thesis, Swedish University of Agricultural Sciences. https://pub.epsilon.slu.se/1956/.

Suh, G. S., Wong, A. M., Hergarden, A. C., Wang, J. W., Simon, A. F., Benzer, S., Axel, R., & Anderson, D. J. (2004). A single population of olfactory sensory neurons mediates an innate avoidance behaviour in Drosophila. *Nature*, *431*(7010), 854–859. https://doi.org/10.1038/nature02980

Tanaka, N. K., Endo, K., & Ito, K. (2012). Organization of antennal lobe-associated neurons in adult Drosophila melanogaster brain. *The Journal of comparative neurology*, *520*(18), 4067–4130. https://doi.org/10.1002/cne.23142

Tauxe, G. M., MacWilliam, D., Boyle, S. M., Guda, T., & Ray, A. (2013). Targeting a dual detector of skin and CO2 to modify mosquito host seeking. *Cell*, *155*(6), 1365–1379. https://doi.org/10.1016/j.cell.2013.11.013

Truman, James W., and Michael Bate. (1988). Spatial and Temporal Patterns of Neurogenesis in the Central Nervous System of *Drosophila melanogaster*. *Developmental Biology* 125 (1): 145–57.

Turner, S. L., & Ray, A. (2009). Modification of CO_2 avoidance behaviour in Drosophila by inhibitory odorants. *Nature*, *461*(7261), 277–281. https://doi.org/10.1038/nature08295

van Breugel, F., Huda, A., & Dickinson, M. H. (2018). Distinct activity-gated pathways mediate attraction and aversion to CO_2 in Drosophila. *Nature*, *564*(7736), 420–424. https://doi.org/10.1038/s41586-018-0732-8

Vilinsky, I., Hibbard, K. L., Johnson, B. R., & Deitcher, D. L. (2018). Probing Synaptic Transmission and Behavior in *Drosophila* with Optogenetics: A Laboratory Exercise. *Journal of undergraduate neuroscience education : JUNE : a publication of FUN, Faculty for Undergraduate Neuroscience*, *16*(3), A289–A295.

Vosshall, L. B., & Stocker, R. F. (2007). Molecular architecture of smell and taste in Drosophila. *Annual review of neuroscience*, *30*, 505–533. https://doi.org/10.1146/annurev.neuro.30.051606.094306

Wagh, D. A., Rasse, T. M., Asan, E., Hofbauer, A., Schwenkert, I., Dürrbeck, H., Buchner, S., Dabauvalle, M. C., Schmidt, M., Qin, G., Wichmann, C., Kittel, R., Sigrist, S. J., & Buchner, E. (2006). Bruchpilot, a protein with homology to ELKS/CAST, is required for structural integrity and function of synaptic active zones in Drosophila. *Neuron*, *49*(6), 833–844. https://doi.org/10.1016/j.neuron.2006.02.008

Wilson, R. I. (2013). Early olfactory processing in Drosophila: Mechanisms and principles. *Annual Review of Neuroscience*, 36, 217–241. https://doi.org/10.1146/annurev-neuro-062111-150533

Winding, M., Pedigo, B. D., Barnes, C. L., Patsolic, H. G., Park, Y., Kazimiers, T., Fushiki, A., Andrade, I. V., Khandelwal, A., Valdes-Aleman, J., Li, F., Randel, N., Barsotti, E., Correia, A., Fetter, R. D., Hartenstein, V., Priebe, C. E., Vogelstein, J. T., Cardona, A., & Zlatic, M. (2023). The connectome of an insect brain. *Science (New York, N.Y.)*, *379*(6636), eadd9330. https://doi.org/10.1126/science.add9330

Wu, Y., Helt, J. C., Wexler, E., Petrova, I. M., Noordermeer, J. N., Fradkin, L. G., & Hing, H. (2014). Wnt5 and drl/ryk gradients pattern the Drosophila olfactory dendritic map. *The Journal of neuroscience : the official journal of the Society for Neuroscience*, *34*(45), 14961–14972. https://doi.org/10.1523/JNEUROSCI.2676-14.2014

Zheng, Z., Lauritzen, J. S., Perlman, E., Robinson, C. G., Nichols, M., Milkie, D., Torrens, O., Price, J., Fisher, C. B., Sharifi, N., Calle-Schuler, S. A., Kmecova, L., Ali, I. J., Karsh, B., Trautman, E. T., Bogovic, J. A., Hanslovsky, P., Jefferis, G. S. X. E., Kazhdan, M., Khairy, K., … Bock, D. D. (2018). A Complete Electron Microscopy Volume of the Brain of Adult Drosophila melanogaster. *Cell*, *174*(3), 730–743.e22. https://doi.org/10.1016/j.cell.2018.06.019

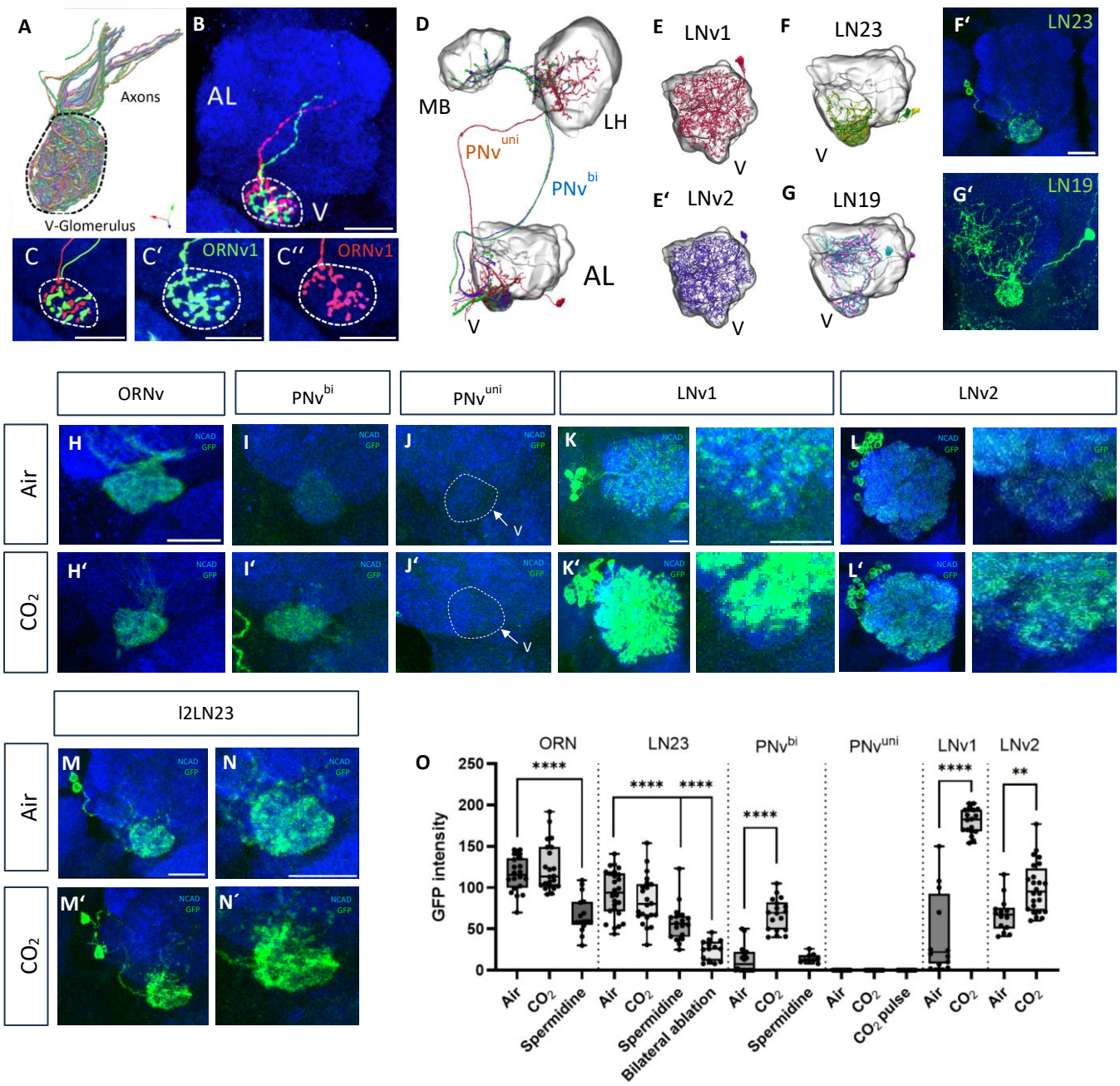

Figure 1. Principal neurons of the V glomerulus show distinct response properties for CO_2. (A–C) About 40 olfactory sensory neurons (ORNv) innervate the ipsilateral V glomerulus at the ventral AL surface (A). Single cell clones revealed the terminal branch pattern of ORNv axons (B). Each ORNv axon forms 3–5 non-overlapping terminal branches (C). **(D–G)** Morphology of central neurons of the V glomerulus, including 2 types of projection neurons (PNv^{uni} and PNv^{bi}, D), 2 classes of broad local interneurons (LNv1 and LNv2, E/E') and 2 classes of sparse LNs (LN23 and LN19, F, G). Gal4 expression lines for sparse interneurons LN23 and LN19 (F', G'). **(H–N)** CaLexA reporter expression in different neuron classes under ambient air (H–N) and elevated CO_2 levels (H'–N'). CaLexA activity could be observed in ORNv, LNv1/2 and LN19, but not in glomerular PNs under ambient air conditions. **(H'-N')** Following chronic CO_2 stimulation, ORNv and LN23 show high activity, comparable to the GFP expression levels at ambient air. Based on the CaLexA-GFP intensity, previous activity was higher for PNv^{bi} following stimulation as was the case for LNv1 and LNv2. PNv^{uni} showed no activity as indicated by the GFP levels. **(O)** Quantification of GFP signal intensity in ORNv, LN23, PNv^{bi}, PNv^{uni}, LNv1, and LNv2. The experimental conditions were, that the flies were either kept in ambient air or in 5% CO_2 for 3 consecutive days. For ORNs, LN23 and PNv^{bi} we also exposed the flies to spermidine, which is a strong GR21a (ORNv) inhibitor. The effect was so strong for LN23, so that we also wanted to compare it to a complete bilateral ablation of both antennae. Further, since continuous exposure to CO_2 did not produce any GFP signal for PNv^{uni}, we tried a pulsed presentation of the CO_2 stimulus, but that also showed no effect. The white bars at the lower right corners indicate the scale of 20 ym. This also applies to the following figures.

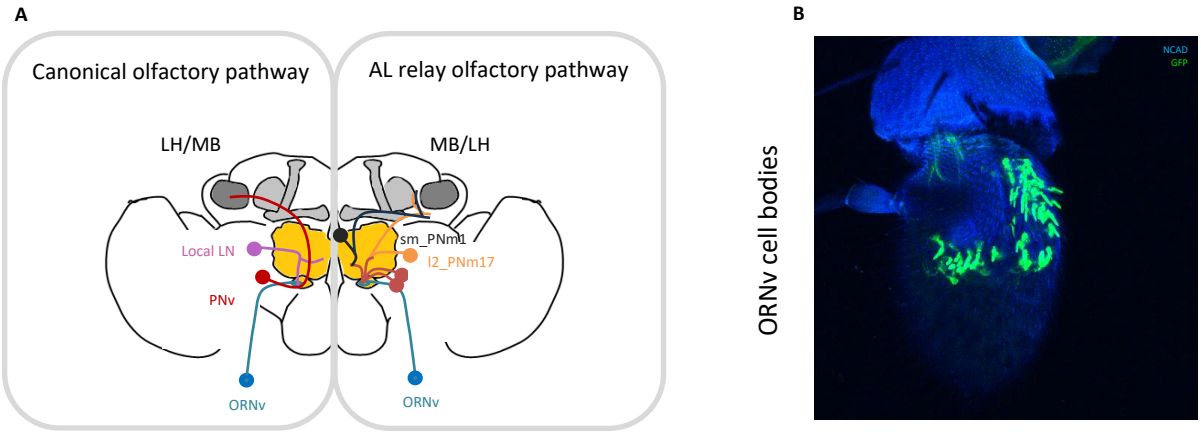

Supplementary Figure 1. (A) Schematic of the canonical olfactory pathway (left) and the identified AL relay pathway (right). **(B)** CaLexA::GFP expression in vORN cell bodies on the 3rd antennal segment.

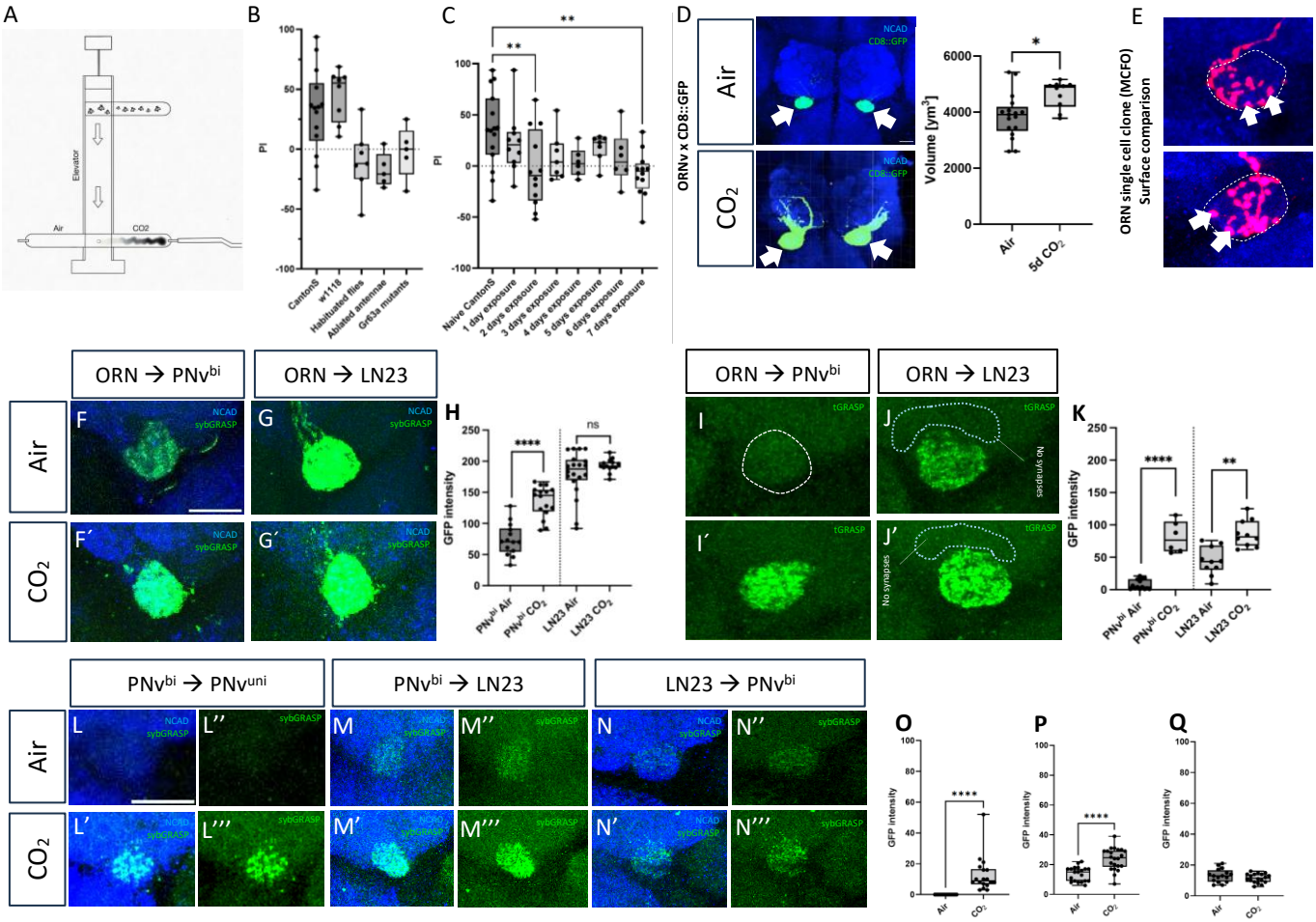

Figure 2. Circuit dynamics of the V glomerulus during CO_2-induced habituation. (A) T-maze setup to determine CO_2 valence identity of adult flies. **(B)** Performance index (PI) of naïve flies compared to flies, which have experienced either chronic CO_2 exposure, removal of both antennae or a mutation of the CO_2 receptor GR63a, each of it leading to a loss of innate aversion response towards CO_2. A value of 100 for the PI represents a 100% attraction towards ambient air for a tested group of flies, while a negative value of -100 would indicate a 100% attraction towards 5% CO_2. **(C)** Temporal pattern of CO_2-induced behavioral habituation. It became evident, that even after 1 day of exposure, that aversion towards 5% CO_2 already decreased drastically. **(D, E)** Structural changes of the V glomerulus volume (D) and axonal arborization of ORNv (E) following 5 days of chronic CO_2 stimulation. **(F–Q)** Synaptic connectivity among neurons of the V glomerulus analyzed by transgenic GRASP. Activity-dependent sybGRASP indicates enhanced ORNv→PNv^{bi} connectivity (F', H), but no significant changes for ORNv→LN23 (G', H) during behavioral habituation. Activity-independent tGRASP expression demonstrates increased synaptic connectivity of ORNv axons with PNv^{bi} and LN23, consistent with morphological changes observed in ORN terminals during habituation (I', J', K). ORN input is restricted to the glomerulus but not seen in the extra-glomerular region (arrows, J).Differences in SybGRASP levels among central neurons of the V glomerulus PNv^{bi} neurons showed higher GFP intensity after prolonged exposure to elevated CO_2 levels (O, P compared to Q). The GFP levels for LN23 remained similar to the ambient air control (L-Q)

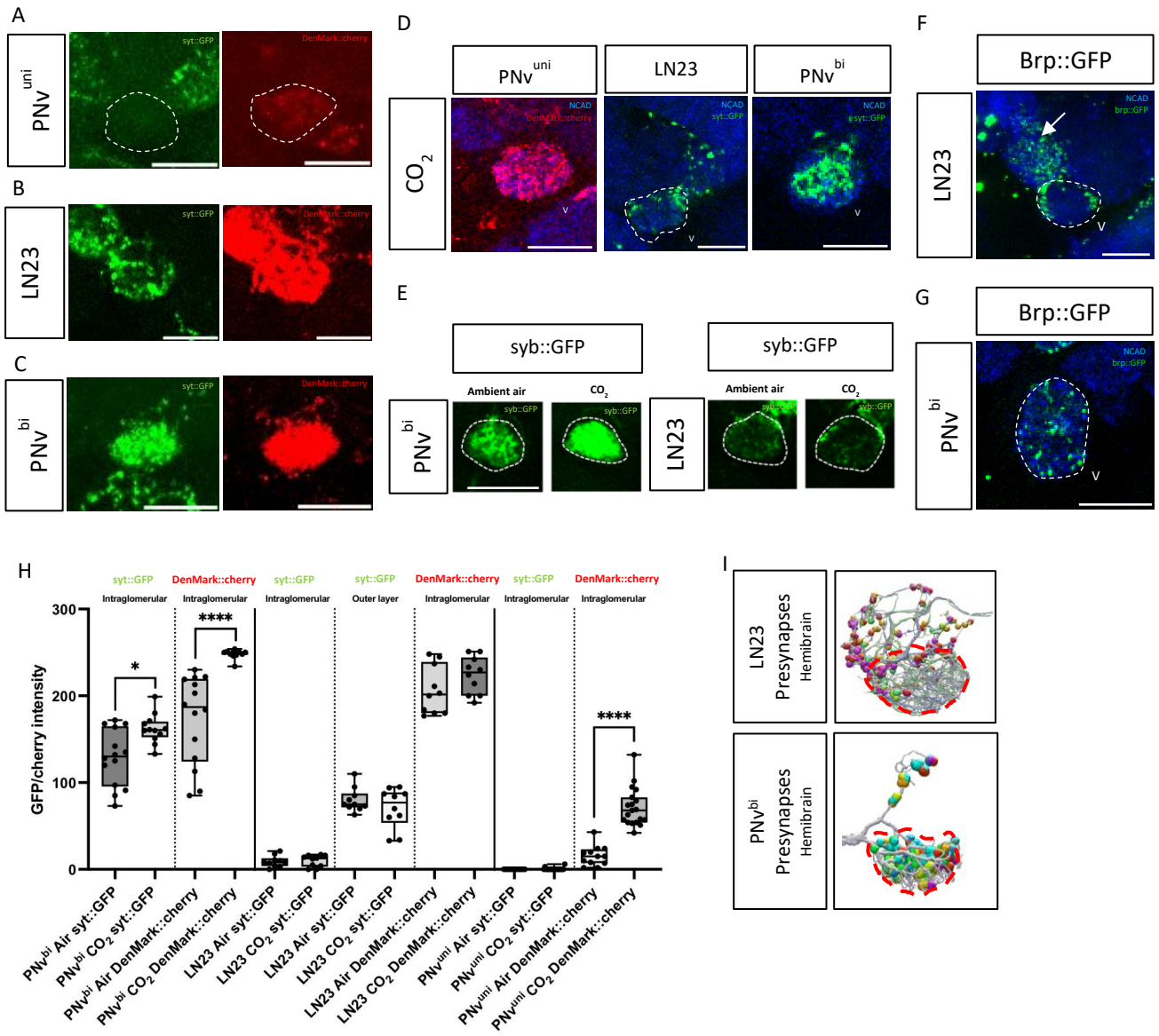

Figure 3. Neuronal polarity of CO_2 glomerular circuit components. (A-C) confocal sections illustrate *syt::GFP* and *DenMark::Cherry* expression in LN23 Quantification of GFP/cherry levels *syt::GFP* and *DenMark::Cherry* revealed distinct localization of presynaptic sites in PNv^{bi}, PNv^{uni}, and LN23. PNv^{bi} displayed prominent presynaptic labeling throughout the glomerular neuropil, while PNv^{uni} showed no detectable presynaptic signal, despite clear dendritic arborizations. LN23 exhibited scattered presynaptic puncta largely outside the glomerular boundaries. **(D)** PNv^{uni} LN23 and PNv^{bi} show different responses following habituation. While LN23 did not show increased *syt::GFP* or *DenMark::cherry* signal, both were increased for PNv^{bi} while for PNv^{uni} only *DenMark::cherry* was amplified . **(E)** *Syb::GFP* labeling further confirmed that presynaptic sites in PNv^{bi} were restricted to the glomerular neuropil and increased after chronic CO_2 exposure, whereas LN23 signals remained scattered along the glomerular margin. **(F-G)** Higher-resolution optical sections confirm the presence of *brp::GFP* puncta in LN23 dendrites outside the V glomerulus **(F, arrow)** but confined to the V glomerulus in PNv^{bi}. **(H)** Quantification of *syt::GFP* and *DenMark::cherry*. For LN23 we differentiated between intensity measurements in the center of the glomerulus and measurements near the glomerular boundary. **(I)** Hemibrain reconstructions show the enrichment of LN23 presynaptic sites (colored spheres) in extraglomerular domains compared to the intraglomerular distribution in PNv^{bi}

A

LN23::GFP

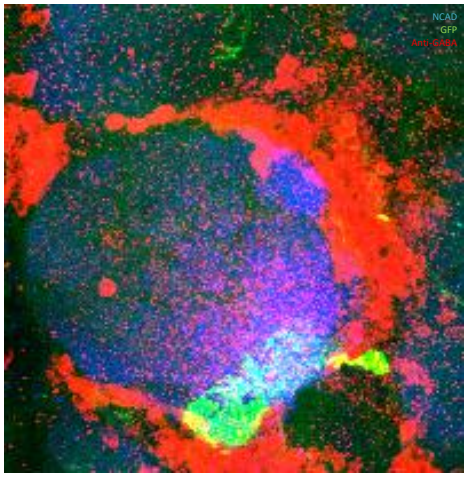

Supplementary Figure 3. (A) CaLexA labeling of LN23 combined with anti-GABA staining revealed no colocalization, indicating that LN23 is not GABAergic.

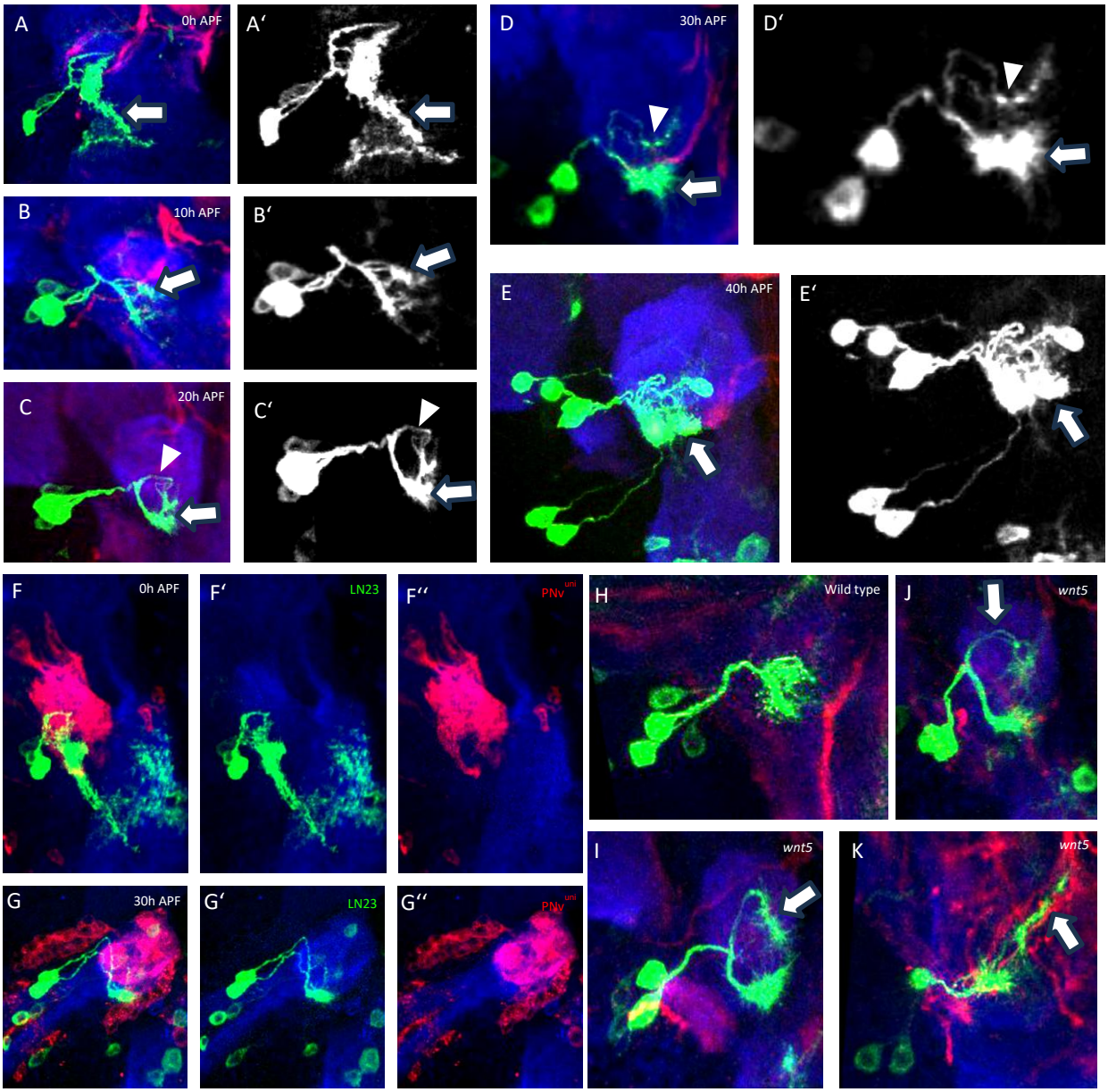

Figure 4. Early LN23 development. (A-E') At the beginning of pupal development (0h APF), larval LN23 neurons remodel their ventral processes (arrow in A) and start extending into the developing adult AL (arrow in B). While a broad arborization can be observed in the ventral AL (arrows in C and D), a small process extends in the dorsal AL to target posterior to the V glomerulus (arrowheads in C and D). At 40h APF, the main LN23 dendrites are restricted to the glomerular boundaries (arrow in E). **(F-G'')** In the reorganization from the larval to adult AL, LN23 processes (green) synchronize with uni-glomerular PN dendrites (red). Compared to wild type **(H)**, loss of *Wnt5* **(I-K)** leads to a larger separation of ventral and dorsal LN23 branches (arrows in I and J), which later extend along axons towards higher brain centers (arrow in K).

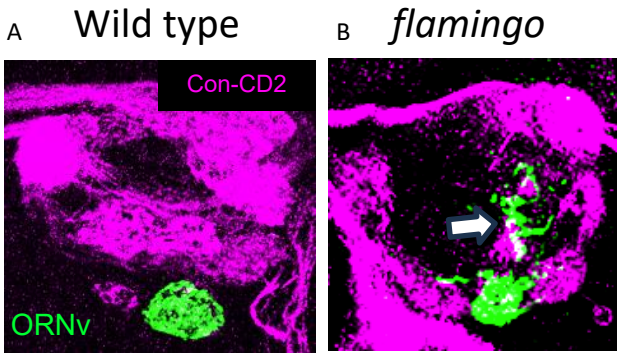

Supplementary Figure 4. Loss of the cell adhesion molecule Flamingo in ORNv. In contrast to the (A) wild type axonal convergence of ORNv within the glomerular boundaries, (B) *fmi*-mutant ORNv axons overshoot the ventral glomerular domain and extend into the posterior AL (arrow).

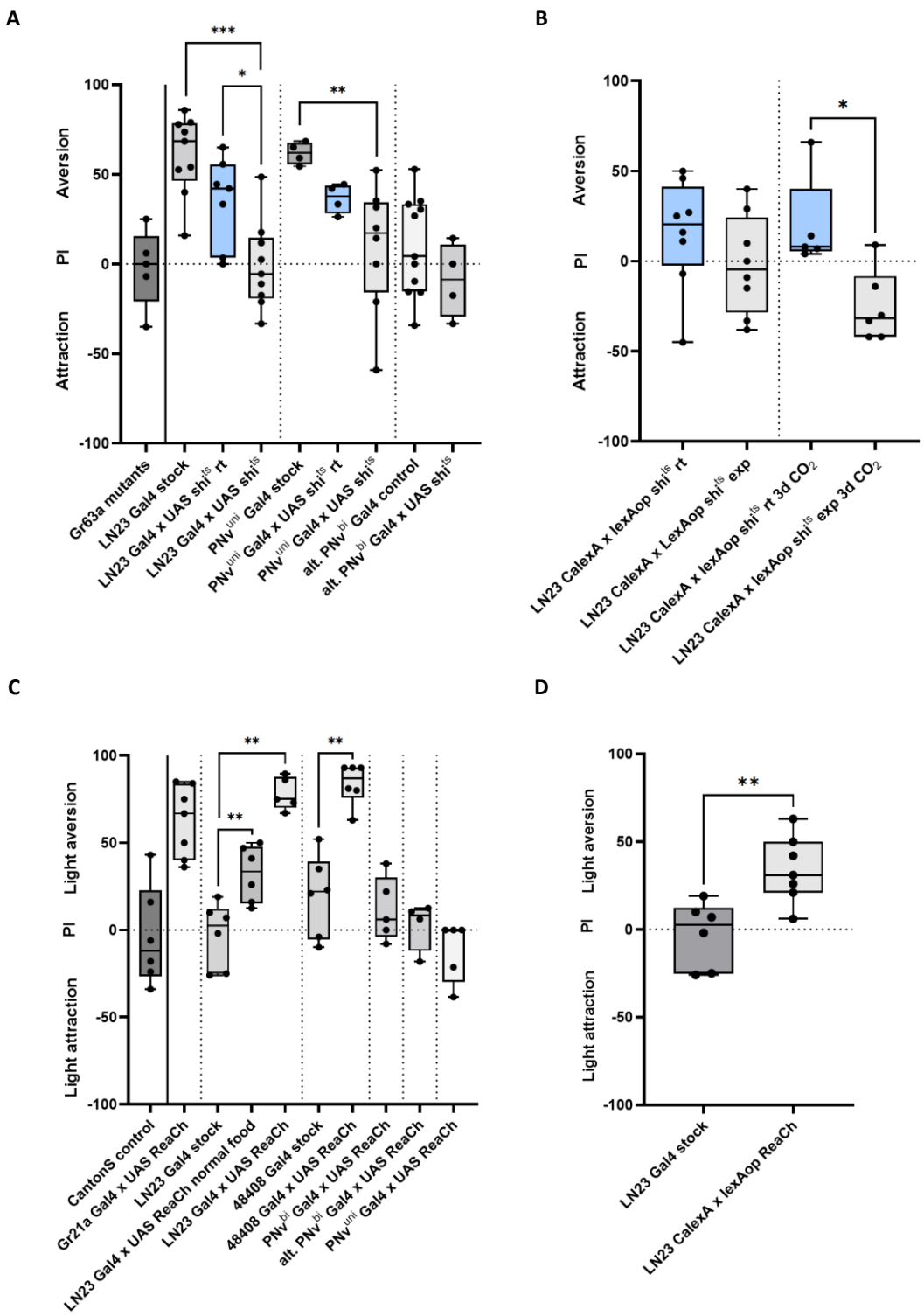

Figure 5. Activity of LN23 controls CO_2 aversion behavior. (A) Cell type–specific silencing with UAS-shibire^{ts} revealed that neuronal activity of all three V-glomerulus relay neurons contributes to innate CO_2 avoidance. Silencing of PNv^{uni} or PNv^{bi} reduced avoidance behavior, with a stronger effect in PNv^{uni}. In contrast, LN23 silencing abolished CO_2 aversion entirely. Control experiments performed at room temperature (rt; exp stands for experimental condition at restrictive temperatures), where shibire^{ts} should remain permissive, showed partial reduction of avoidance in PNv^{uni} and LN23. Since experiments with PNv^{bi} Gal4 (VT031497) showed inconclusive results, we used the alternative PNv^{bi} (alt. PNv^{bi}) Gal4 driver line (R53A05; BDSC#38859). **(B)** Cell type–specific expression of shibire^{ts} via CaLexA confirmed the essential role of LN23 in CO_2 behavior. LN23 CaLexA-shibire^{ts} flies showed reduced avoidance, and chronic CO_2 exposure, which should boost CaLexA activity, shifted behavior from avoidance to attraction. **(C)** Optogenetic activation using UAS-ReaChR demonstrated sufficiency of LN23 for driving aversive behavior. Light activation of ORNv (GR21a-Gal4) and LN23 (independent drivers LN23-Gal4 and alternative line 48408-Gal4) triggered robust avoidance, while activation of PNv^{bi} or PNv^{uni} failed to elicit significant changes. **(D)** CaLexA-driven ReaChR expression in LN23 also induced light-mediated aversion, confirming cell type specificity.

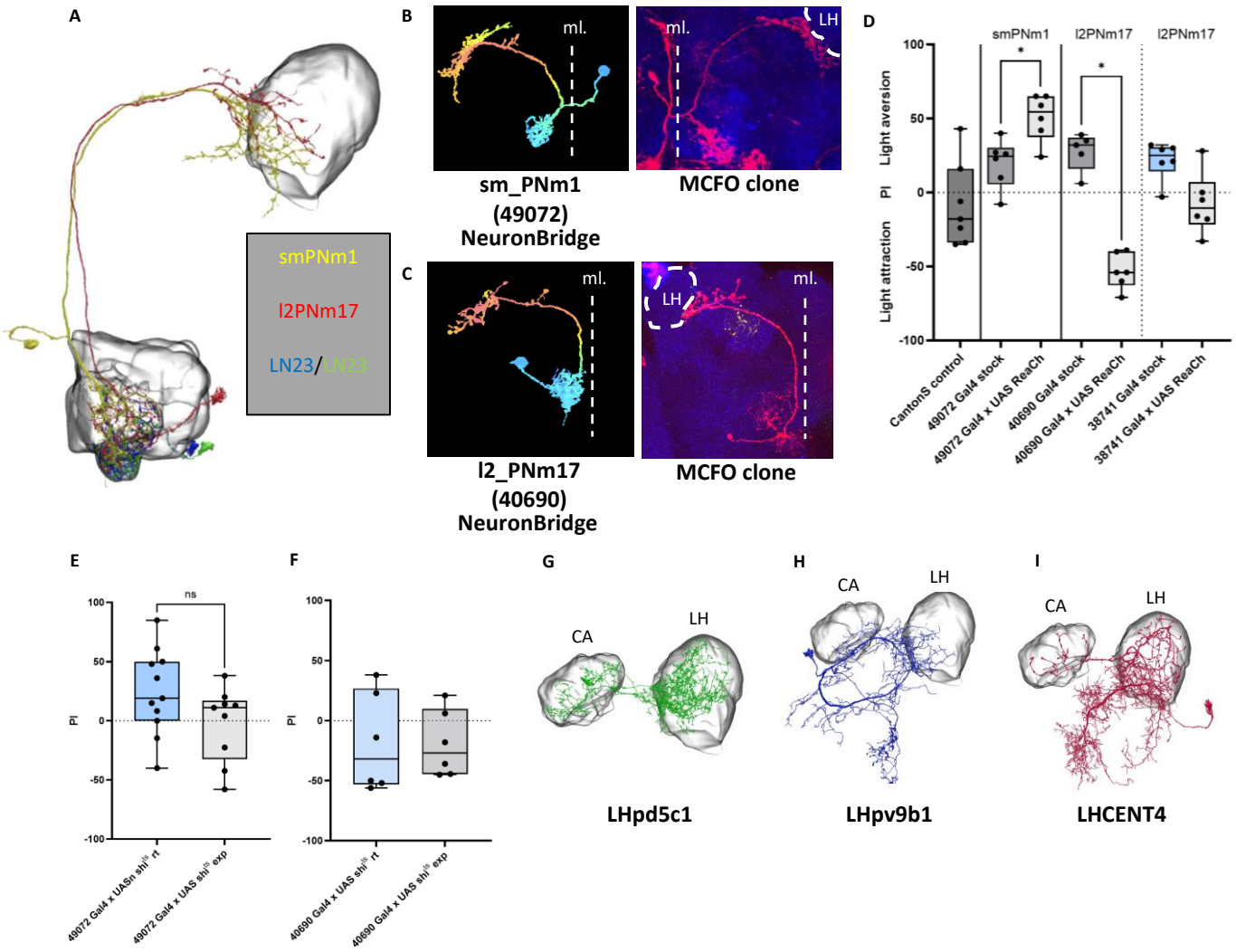

Figure 6. Two postsynaptic neurons of LN23 convey opposing odor valance. (A) Connectomic analysis (neuPrint, Janelia Research Campus) revealed two major postsynaptic partners of LN23, PNm1 and PNm17. **(B, C)** Single-cell MCFO clones of sm_PNm1 and l2_PNm17 show axonal projections bypassing the canonical olfactory lateral horn (LH) and targeting adjacent regions including the posterior lateral protocerebrum (PLP), superior clamp (SCL), and superior lateral protocerebrum (SLP). **(D)** Optogenetic activation of PNm1 induced strong aversion, whereas PNm17 activation elicited attraction, demonstrating opposing behavioral valence. **(E, F)** Silencing experiments with shibire^{ts} confirmed that CO_2 aversion requires PNm1 activity but is unaffected by PNm17 silencing. **(G–I)** Hemibrain connectome data identified distinct downstream LH partners for the two CO_2 relay pathways: LHPD5c1 as the primary postsynaptic target of PNv^{bi}, LHPV9b1 downstream of PNm1, and LHCENT4 downstream of PNv^{uni}. The abbreviation "rt" stands for the room temperature control of shibirets while "exp" is the experimental condition at the restrictive temperature. The midline in the brain is indicated by the dashed line and "ml.".

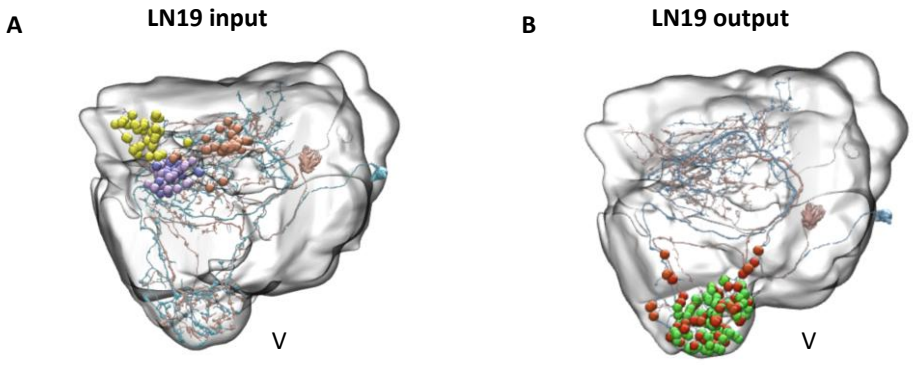

C

Postsynaptic partner	# of connections		Presynaptic partners	# of connections
PNv^{bi}	223		ORNv	292
ORNv	201		ORN_VM7v	128
vLN24	158		VM7d_adPN	91
VM7d_adPN	140		ORN_DC4	72
PNv^{uni}	134		DM4_adPN	43

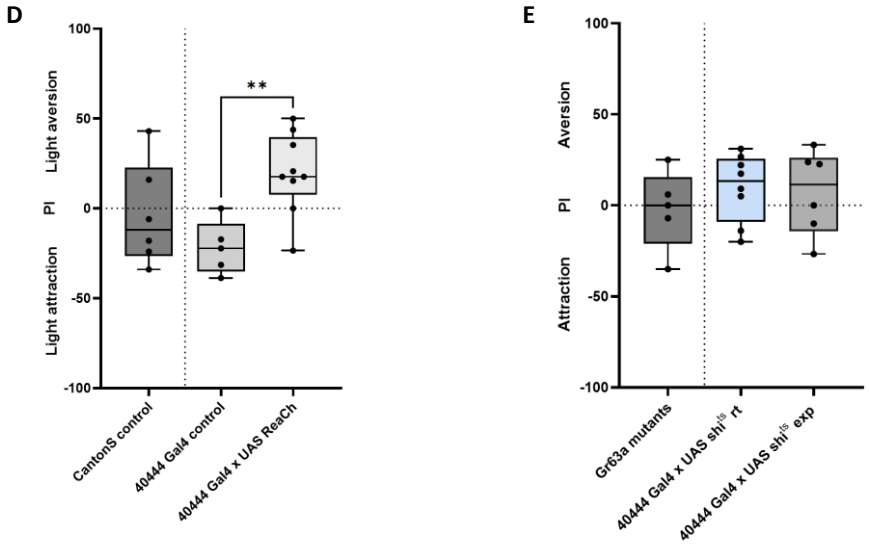

Figure 7. The "food" odor associated l2LN19. (A) LN19 gets input from DM4, DC4/DP1 and VM7 while **(B)** the output is within the V glomerulus. **(C)** Table illustrating the post,- and presynaptic partners of LN19 as they can be found on https://neuprint.janelia.org/ **(D)** Optogenetic activation of LN19 using a specific driver line induced strong behavioral aversion, indicating that LN19 activity can bias olfactory responses towards avoidance. **(E)** In contrast, silencing LN19 via shibire^{ts} did not alter innate CO_2 avoidance, suggesting that while LN19 is sufficient to promote aversive responses, it is not essential for baseline CO_2-driven behavior. The abbreviation "rt" stands for the room temperature control of shibire^{ts} while "exp" is the experimental condition at the restrictive temperature.

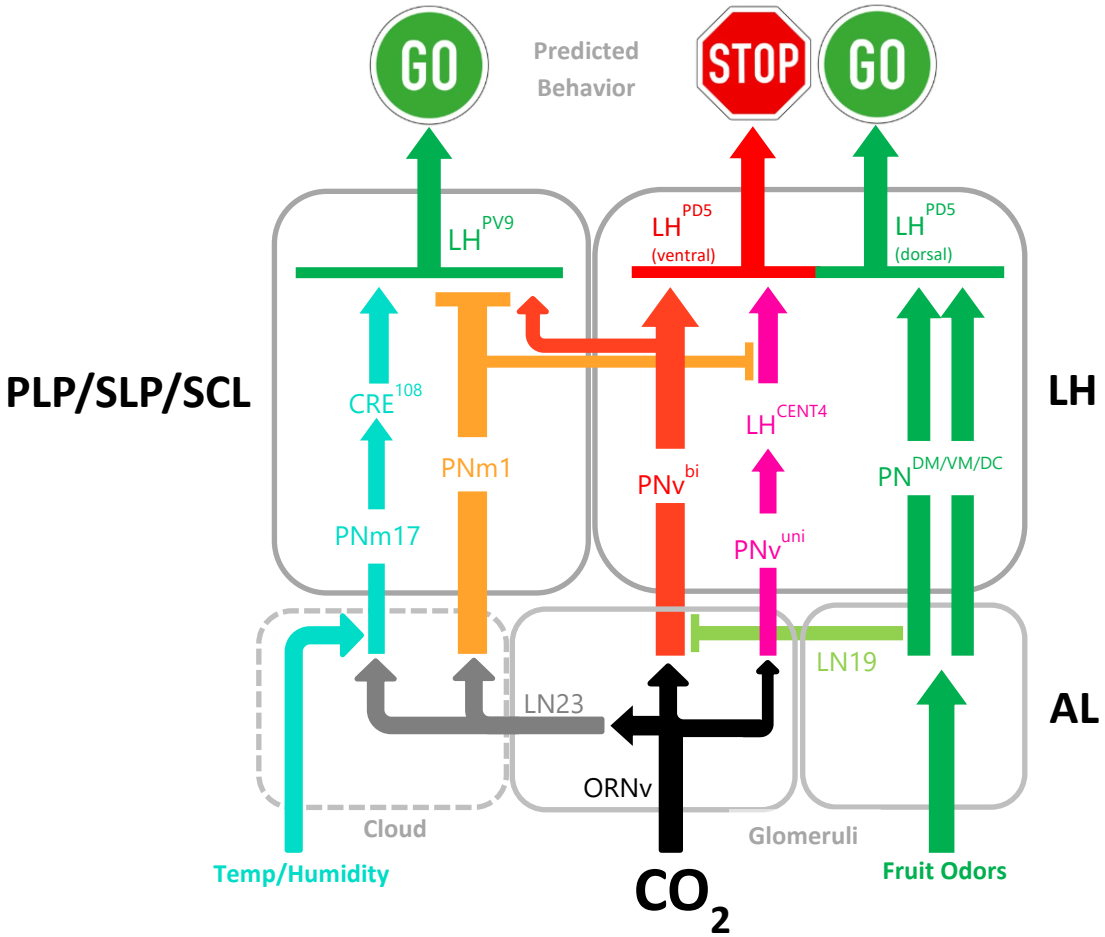

Figure 8. Convergence of parallel channels for CO_2 valence coding. The activity of CO_2-responsive sensory neurons (ORNv, black) is relayed by 4 parallel PN channels to converge onto 2 central brain target neurons of opposite intrinsic valence identity. First, the glomerular PNv^{bi} (red) and PNv^{uni} (pink) target the ventral domain of LH^{PD5} (directly or via LN^{cent4}, respectively) to trigger behavioral aversion (red). Second, the extraglomerular PNm1 (yellow) and PNm17 (turquoise), activated via the lateral LN23 relay (grey), converge onto LH^{PV9} (directly or via CRE^{108}, respectively) which mediates attraction (green). While PNm17 supports LH^{PV9} activity, GABAergic PNm1 blocks LH^{PV9} thereby resulting in an aversive response. This core aversion domain (PNv^{bi}/PNv^{uni}/PNm1) can be modified either via the activation of the dorsal LH^{PD5} domain by fruit odor PNs ($PN^{DM/VM/DC}$, green) or an increase of PNm17 by non-olfactory sensory neurons (turquoise). PNv^{bi} is providing balancing activity between channels, for example through direct input onto LH^{PV9} or via receiving LN19-mediated inhibition by food PNs.